Geosci. Model Dev. Discuss., 7, 8805–8873, 2014
www.geosci-model-dev-discuss.net/7/8805/2014/
doi:10.5194/gmdd-7-8805-2014

Geoscientific Model Development Discussions
Open Access

Normal-mode function representation of global 3-D datasets: an open-access software for atmospheric research community

N. Žagar[1], A. Kasahara[2], K. Terasaki[3], J. Tribbia[2], and H. Tanaka[3]

[1]University of Ljubljana, Ljubljana, Slovenia
[2]National Center for Atmospheric Research, Boulder, Colorado, USA
[3]University of Tsukuba, Tsukuba, Japan

Received: 21 October 2014 – Accepted: 10 November 2014 – Published: 10 December 2014

Correspondence to: N. Žagar (nedjeljka.zagar@fmf.uni-lj.si)

Published by Copernicus Publications on behalf of the European Geosciences Union.

Abstract

The paper presents new software for the analysis of global dynamical fields in (re)analyses, weather forecasts and climate models. A new diagnostic tool, developed within the MODES project, allows one to diagnose properties of balanced and inertio-gravity (IG) circulation across many scales. In particular, the IG spectrum, which has only recently become observable, can be studied simultaneously in the mass field and wind field and considering the whole model depth in contrary to majority of studies.

The paper presentation includes the theory of normal-mode function expansion, technical details of the Fortran 90 code, examples of namelists which control the software execution and outputs of the software application on the reanalysis dataset ERA Interim. The applied libraries and default compiler are from the open-source domain. A limited understanding of Fortran suffices for the successful implementation of the software.

The presented application of the software to the ERA Interim dataset show some features of the large-scale circulation after it has been split into the balanced and IG components. The global energy distribution is dominated by the balanced energy with IG modes making less than 10 % of the total wave energy. However, on subsynoptic scales IG energy dominates and it is associated with the main features of tropical variability on all scales. The presented energy distribution and features of the zonally-averaged and equatorial circulation provide a reference for the validation of climate models.

1 Introduction

Spherical harmonics have been used extensively for representing many geophysical quantities over the globe. They are useful for the decomposition of global circulation data also because they are eigensolutions of the global barotropic vorticity equation. Furthermore, spherical harmonics are used as basis functions for the numeri-

GMDD
7, 8805–8873, 2014

cal discretization of dynamical terms of the global prognostic equations for numerical weather prediction (NWP) in some of major global NWP models (e.g. ECMWF). A scale-dependent distribution of atmospheric kinetic energy at a given horizontal level is readily produced from spherical harmonics as a function of the global wavenumber (e.g. Boer and Shepherd, 1983).

It is however often more desirable to represent flow patterns not only of the horizontal velocity components but also of the associated mass field variables as functions of longitude, latitude, and height. Since our picture of the atmosphere is that of a vibrating system with many modes of oscillations, like a musical instrument, it is desirable to have some vector functions to represent simultaneously both wind field and mass field corresponding to the various modes. Such modes are provided by the eigensolutions of the linearized governing (or primitive) equations, and they are known as normal modes.

It is the objective of this article to present the development and application of a software that applies 3-D vector harmonic functions based on the natural modes of oscillations for representing global circulation patterns in terms of a single expansion series. The presented development of 3-D vector functions is based on the theoretical work by Kasahara and Puri (1981). They derived the set of three-dimensionally orthogonal normal mode functions (NMFs) and applied it on the hemispheric data from the NCEP system. The orthogonal expansion basis was derived for the vertical σ coordinate which is naturally suited for the representation of data on the Earth.

The derivation of NMFs by Kasahara and Puri (1981) was not utilized until Žagar et al. (2009a) applied the method for the comparison of levels of inertio-gravity energy in modern analysis datasets on model levels. Several other recent papers applied the method for the diagnosis of data assimilation systems, especially their balance properties and the scale-dependent properties of short-range forecast errors (Žagar et al., 2011, 2012, 2013).

A more extensive work based on the application of NMFs has been carried out in the pressure system. Tanaka (1985) and Tanaka and Kung (1988) derived a 3-D normal-mode scheme for the pressure vertical coordinate. The method was applied for

GMDD
7, 8805–8873, 2014

a number of research topics ranging from baroclinicity (Kasahara and Tanaka, 1989) and blocking (Tanaka and Terasaki, 2006) to global energetics and energy conversion studies (Tanaka and Kimura, 1996; Marques and Castanheira, 2012). In the case of pressure system, global circulation is represented by winds and geopotential on 10 to 20 standard pressure levels.

The most important application of normal modes in NWP research has been the initialization of operational forecast models, known as the non-linear normal-mode initialization (NNMI) (Baer and Tribbia, 1977; Machenhauer, 1977; Wergen, 1988; Errico, 1997). With the advance of modern data assimilation methodologies such as 4-D-Var (e.g. Le Dimet and Talagrand, 1986) and the application of digital filtering for initialization (e.g. Lynch and Huang, 1992) the use of NNMI has greatly reduced. One of more recent applications of NNMI is within the NCEP global NWP system (Kleist et al., 2009). We also note that sets of normal modes derived for the initialization of NWP models were not 3-D orthogonal.

On the other hand, the global horizontal structures of normal modes, known as Hough functions, have been used to analyze atmospheric variability (Madden, 2007, and references therein). Some fundamental properties of the large-scale tropical circulation in both the atmosphere and the ocean have been described in terms of normal modes on the equatorial-β plane (e.g. Gill, 1980). The equatorial Kelvin, the mixed Rossby-gravity and the equatorially trapped inertio-gravity and Rossby modes characterized by small phase speeds have been associated with the most energetic modes of tropical variability in direct or derived observations and in weather and climate models. Wave properties have been diagnosed by using mass-field information such as the outgoing longwave radiation (e.g. Wheeler and Kiladis, 1999), brightness temperature (e.g. Yang et al., 2003), precipitation (e.g. Kim and Alexander, 2013) or climate models (e.g. Lin et al., 2006). In contrary to these studies based on spectral-temporal filtering, the representation of global data in terms of normal modes represents temperature field and wind field simultaneously in terms of balanced (quasi-rotational) and

GMDD
7, 8805–8873, 2014

unbalanced (eastward- and westward-propagating inertio-gravity) motions of different vertical and horizontal scales.

A separation of nonlinear atmospheric motions into the high-frequency inertio-gravity and low-frequency balanced motions is possible only if the simplification of linearized equations around some specific background states is introduced. Furthermore, the vertical part of solutions can be obtained analytically only for some special cases such as the isothermal atmosphere (Daley, 1991, Chapter 6) or a constant stability profile (e.g. Terasaki and Tanaka, 2007). For realistic temperature and stability profiles, solutions need to be obtained numerically and numerical procedures for the solution of the vertical structure of global normal modes have been considered in several papers (e.g. Kasahara and Puri, 1981; Kasahara, 1984; Staniforth et al., 1985).

The 3-D orthogonality of normal modes allowed Kasahara and Puri (1981) to estimate the contribution of inertio-gravity modes to the total *wave* (zonal wavenumber > 0) energy; they found that the percentage of total wave energy associated with the inertio-gravity modes was small. Such a result was in agreement with the quasi-geostrophic scaling and a poor quality of the tropical analyses in late 1970s. It agreed also with a study by Daley (1983) that estimated an average percentage of ageostrophic motions in early analyses of ECMWF to be about 10 % implying that about 1 % of atmospheric wave energy was associated with unbalanced flows. Thirty years later, data assimilation methodology and an unprecedented amount of high-quality atmospheric observations provide us with the most reliable picture of global circulation we have ever had. In particular, reanalysis datasets (e.g. Dee et al., 2011) are used to validate atmospheric variability represented by climate models in support to their simulation of climate scenarios for the future.

In relation to a more reliable representation of physical processes in later analyses, especially convection, and associated divergent circulation Žagar et al. (2009a) reported that the level of IG energy is about 10 % of the total wave energy; in other words, in current analysis datasets about one-third of global variability is associated with unbalanced circulation. Realistic climate models validated against (re)analyses should be

GMDD
7, 8805–8873, 2014

characterized by a similar amount of unbalanced energy and its scale distribution. The application of 3-D normal modes presented in this paper provides a picture of the unbalanced component of the global circulation in the latest reanalyses of ECMWF, ERA Interim dataset (Dee et al., 2011).

In what follows, we present details of the software for NMF analysis and describe a sequence of steps applied to generate a picture of the unbalanced component of global circulation in ERA Interim reanalyses. The application of the software is controlled through the namelists which are provided in Appendix. It is shown that a moderate user effort suffices for the application of the software to other global datasets. In particular, we discuss the choice of several namelist parameters and outline the future directions of the software development. The most important direction is the comparison of energy distribution in reanalyses and climate simulations of the present-day climate followed by the comparison of the simulated present-day unbalanced circulation and its projections. Most of the unbalanced large-scale planetary and synoptic-scale circulation is found in the tropics. At the same time, tropics is the region of largest uncertainties in both short-range forecasts (e.g. Žagar et al., 2013) and in climate models (e.g. Lin et al., 2006). Evaluation of models' ability to reproduce the unbalanced tropical circulation can be expected to provide a new insight on models' performance that is helpful to diagnose models' deficiencies and define improvements.

The paper is structured as follows: The next section presents the theory of normal modes as an updated extended summary of the article by Kasahara and Puri (1981), hereafter denoted KP1981. Section 3 provides step-by-step description of various components of the normal mode software which can be followed by the user interested to implement the software. In Sect. 4 we present outputs of the normal-mode diagnostics of ERA Interim by using a few standard diagnostics. Summary and conclusions are provided in Sect. 5. Several appendices contain examples of namelists which are edited by a user to run the software.

GMDD
7, 8805–8873, 2014

2 Derivation of 3-D normal mode functions

The derivation of 3-D normal modes presented in this section follows KP1981 although the notation is somewhat different. The reader is also referred to several other cited papers for any missing details.

2.1 Model of the atmosphere

As a model of the atmosphere, we deal with the traditional hydrostatic baroclinic primitive equation system on a sphere, customarily adopted for numerical weather prediction (Kasahara, 1974). The model describes the time evolution of eastward and northward velocity components (u', v') and geopotential height as functions of longitude, λ, latitude, φ, vertical coordinate, σ, and time t. The σ coordinate is defined by

$$\sigma = \frac{p}{p_s}, \tag{1}$$

where p and p_s denote the pressure and surface pressure, respectively (Phillips, 1957).

Although the atmospheric model is nonlinear, we are interested in small-amplitude motions around the basic state of atmosphere at rest. Therefore, we can deal with a linearized adiabatic and inviscid version of the model. Solutions of such a system with appropriate boundary conditions are referred to as normal modes (Lamb, 1932). It should be noted that we are dealing with free oscillations instead of forced oscillations such as atmospheric tides (Chapman and Lindzen, 1970).

A new geopotential variable introduced by KP1981 accounts for the fact that the surface pressure p_s varies and it is defined as

$$P = \Phi + RT_0 \ln(p_s), \tag{2}$$

where $\Phi = gz$. Here, z denotes the height corresponding to the hydrostatic pressure and g the Earth's gravity. Also, $T_0(\sigma)$ denotes the globally averaged temperature at

GMDD
7, 8805–8873, 2014

a given σ level and R the gas constant of air. It is convenient to introduce a modified geopotential height $h' = P/g$ in the subsequent development.

The system of linearized equations describing oscillations (u', v', h') superimposed on a basic state of rest with temperature T_0 as a function of σ takes the following form:

$$\frac{\partial u'}{\partial t} - 2\Omega v' \sin(\varphi) = -\frac{g}{a\cos(\varphi)}\frac{\partial h'}{\partial \lambda}, \tag{3}$$

$$\frac{\partial v'}{\partial t} + 2\Omega u' \sin(\varphi) = -\frac{g}{a}\frac{\partial h'}{\partial \varphi}, \tag{4}$$

$$\frac{\partial}{\partial t}\left[\frac{\partial}{\partial \sigma}\left(\frac{g\sigma}{R\Gamma_0}\frac{\partial h'}{\partial \sigma}\right)\right] - \nabla \cdot \boldsymbol{V}' = 0. \tag{5}$$

Here, a is the Earth's radius and Ω is the Earth's rotation rate. Equation (5) is obtained as a combination of the continuity and thermodynamic equations after the change of variable and by using the suitable boundary conditions. For details see KP1981. The boundary conditions for the system of Eqs. (3)–(5) are

$$g\frac{\partial h'}{d\sigma} = \text{finite at } \sigma = 0, \tag{6}$$

$$g\frac{\partial h'}{d\sigma} + \frac{g\Gamma_0}{T_0}h' = 0 \text{ at } \sigma = 1. \tag{7}$$

The static stability parameter Γ_0 is defined as

$$\Gamma_0 = \frac{\kappa T_0}{\sigma} - \frac{\mathrm{d}T_0}{\mathrm{d}\sigma}, \tag{8}$$

and it is a function of the globally averaged temperature on σ levels, T_0, its vertical gradient and σ.

As inferred from the work of Taylor (1936), the 3-D linearized model (3)–(5) can be solved by the method of separation of the variables. It means that the vector of 3-D

GMDD
7, 8805–8873, 2014

model variables $[u', v', h']^{\mathrm{T}}$ as functions of $(\lambda, \varphi, \sigma)$ and time t is represented as the product of 2-D motions and the vertical structure function $G(\sigma)$:

$$[u', v', h']^{\mathrm{T}}(\lambda, \varphi, \sigma, t) = [u, v, h]^{\mathrm{T}}(\lambda, \varphi, t) \times G(\sigma). \quad (9)$$

Two systems of equations governing three-dimensional motions are connected by particular values of a separation parameter D which is called the equivalent height following Taylor (1936). It turns out that the governing system of the two-dimensional functions is identical in form with the global shallow water equations having the water depth of equivalent height, D. This system is also known as the Laplace Tidal Equations without forcing.

2.2 Vertical structure equation

We first discuss the vertical structure functions $G(\sigma)$ governed by the vertical structure equation (VSE). Solutions of the VSE were first investigated by physicists in connection with the theory of atmospheric tides under various basic state temperature profiles and upper boundary conditions. For the tidal problems, however, solutions of VSE are calculated under specified tide generating mechanisms with a prescribed value of equivalent height corresponding to a given wave frequency. In contrast, for normal mode problems, solutions of VSE are sought for free oscillations (no forcing and dissipation) that determine the values of equivalent height and corresponding vertical functional profiles. During the late 1960's Jacobs and Wiin-Nielsen (1966) and Simons (1968) for example investigated solutions of the VSE in pressure-coordinates based on quasi-geostrophic modelling. Since then many investigators have examined the various aspects of VSE and its solutions as we shall summarize them briefly in the following.

The vertical structure function $G(\sigma)$ is a solution of the VSE written in the dimensionless form as

$$\frac{\mathrm{d}}{\mathrm{d}\sigma}\left(\frac{\sigma}{S}\frac{\mathrm{d}G}{\mathrm{d}\sigma}\right) + \frac{H_*}{D}G = 0, \quad (10)$$

GMDD
7, 8805–8873, 2014

where $S(\sigma) = R\Gamma_0/(gH_*)$. Here, H_* is a scaling constant with the dimension of height, $H_* = 8\,\mathrm{km}$, and R and g are the gas constants of air and gravity, respectively. We assume that $S > 0$ for the stable stratification. A typical profile of S is shown in Fig. 2c in the next section. The equivalent height is denoted by D.

Solutions of the VSE are sought under the boundary conditions that no mass transport takes place through the Earth's surface and the model top. They are represented by

$$\frac{\mathrm{d}G}{\mathrm{d}\sigma} + rG = 0 \text{ where } r = \frac{\Gamma_0}{T_0} \text{ at the bottom } \sigma = 1\,, \tag{11}$$

$$\sigma\frac{\mathrm{d}G}{\mathrm{d}\sigma} = 0 \text{ at the model top } \sigma = \sigma_T\,. \tag{12}$$

Together with homogeneous boundary conditions (11) and (12), the VSE (10) constitutes a Sturm-Liouville problem (Hildebrand, 1958) and its properties are well-known. For example, solutions of Eq. (10) exist only for a set of positive values of equivalent height D as the eigenvalues, and the corresponding solutions, called the eigenfunctions, are orthogonal in the sense that

$$\int_{\sigma_T}^{1} G_i(\sigma)G_j(\sigma)\mathrm{d}\sigma = \delta_{ij}\,, \tag{13}$$

where $\delta_{ij} = 1$ if $i = j$ and zero otherwise.

In the atmosphere with a realistic temperature profile, there is always one discrete solution of Eq. (10), called the *external* or the *Lamb* mode, with the value of D being approximately 10 km. Its corresponding structure function has the largest vertical scale with no zero crossing point in the vertical. Thus this mode represents a vertically averaged motion and it is often referred to as barotropic mode. In addition to this gravest mode there is a continuous or discrete spectrum of *internal* modes depending on upper boundary conditions with varying values of D all smaller than that of the external

GMDD
7, 8805–8873, 2014

mode. The structure functions corresponding to the internal modes have various zero crossing points on the vertical axis. In the next section examples of VSFs for ERA Interim dataset are discussed in details. The spectrum characteristics of VSE solutions have been investigated extensively. For example, Cohn and Dee (1989) showed that the nature of the mode spectrum depends only on the behavior of the coefficients of VSE near the top of model atmosphere.

With the objective to construct the 3-D normal mode functions to represent global atmospheric motions, we need to account for both internal modes as well as the external mode. Moreover, we need to choose the boundary conditions that yield a discrete spectrum of internal modes by using the same top boundary condition as adopted for NWP and climate models which we analyze. Thus, we can represent the spectrum of D in the following order,

$$D_1 > D_2 > D_3 > \ldots > D_m > 0\,, \tag{14}$$

where the integer subscript m can be chosen as large as one wishes to calculate depending on the solution method. The maximal number of vertical modes that can be resolved (i.e. maximal value of m) is determined by the available vertical resolution (i.e. effective number of vertical grid points). In other words, when applied to NWP and climate models, the appropriate set of vertical structure functions is determined by the corresponding boundary conditions and models' vertical resolution.

The case of $m = 1$ is the lowest mode which is the *external mode* corresponding to the largest equivalent height D_1 and its eigenfunction G_1 has no zero-crossing point in its profile. The remaining cases of $m \geq 2$ are referred to as the *internal modes* and G's have $m - 1$ zero-crossing (nodal) points. Vertical structure functions for several modes computed for ERA Interim vertical coordinate are shown in Fig. 4. Details of their numerical calculation are presented in Sect. 3.

GMDD
7, 8805–8873, 2014

The structure functions $G_m(\sigma)$, which are normalized and orthogonal, are said to be complete in the sense that a well-behaved function $f(\sigma)$ can be represented by a series,

$$f(\sigma) = \sum_{m=1}^{\infty} C_m G_m(\sigma), \quad (\sigma_T < \sigma < 1), \tag{15}$$

where the coefficients C_m can be obtained from the inverse transform

$$C_m = \int_{\sigma_T}^{1} f(\sigma) G_m(\sigma) \mathrm{d}\sigma \tag{16}$$

with the aid of the orthogonality condition (13). In reality we use a finite number of modes to represent $f(\sigma)$.

2.3 Horizontal structure equations

After the 3-D model is decomposed into the product of 2-D system and the VSE as done by Eq. (9), we have m systems of horizontal structure equations (HSE) corresponding to m equivalent heights, D_m, as the eigenvalues of VSE (10). The HSEs are identical to linearized global shallow water equations with the depth D_m, sometimes referred to as the barotropic primitive equations. In the following presentation, we drop the subscript m for simplicity, but actually we are dealing with m systems of HSEs describing oscillations around a background state.

To write down the HSEs, we make the dependent variables (u, v, h) and time t dimensionless as

$$\widetilde{u} = \frac{u}{\sqrt{gD}}, \quad \widetilde{v} = \frac{v}{\sqrt{gD}}, \quad \widetilde{h} = \frac{h}{D}, \quad \widetilde{t} = 2\Omega t. \tag{17}$$

Then, the HSEs are written as

$$\frac{\partial}{\partial t}\boldsymbol{W} + \mathbf{L}\boldsymbol{W} = 0, \tag{18}$$

GMDD
7, 8805–8873, 2014

where $\boldsymbol{W}$ denotes the vector dependent variable

$$\boldsymbol{W} = (\widetilde{u}, \widetilde{v}, \widetilde{h})^{\mathrm{T}} \tag{19}$$

and $\mathbf{L}$ is the linear differential matrix operator

$$\mathbf{L} = \begin{vmatrix} 0 & -\sin(\varphi) & \frac{\gamma}{\cos(\varphi)}\frac{\partial}{\partial\lambda} \\ \sin(\varphi) & 0 & \gamma\frac{\partial}{\partial\varphi} \\ \frac{\gamma}{\cos(\varphi)}\frac{\partial}{\partial\lambda} & \frac{\gamma}{\cos(\varphi)}\frac{\partial}{\partial\varphi}[\cos(\varphi)()] & 0 \end{vmatrix}, \tag{20}$$

in which γ is a dimensionless parameter defined as the ratio of shallow-water gravity wave speed and twice the rotation speed of Earth:

$$\gamma = \frac{\sqrt{gD}}{2a\Omega}. \tag{21}$$

Since Eq. (18) is a linear system with respect to time, the solution $\boldsymbol{W}$ can be expressed in terms of harmonics in time as

$$\boldsymbol{W}(\lambda, \varphi, \widetilde{t}) = \boldsymbol{H}_n^k(\lambda, \varphi)\, e^{-i\nu_n^k \widetilde{t}}, \tag{22}$$

where $\boldsymbol{H}_n^k(\lambda, \varphi)$ represents the horizontal structure functions with zonal wavenumber k and meridional index n. The corresponding dimensionless frequency ν_n^k also depends on k and n.

Now, we define the global inner product as

$$\langle \boldsymbol{W}_p, \boldsymbol{W}_r^* \rangle = \frac{1}{2\pi} \int_0^{2\pi} \int_{-1}^{1} \left(\widetilde{u}_p \widetilde{u}_r^* + \widetilde{v}_p \widetilde{v}_r^* + \widetilde{h}_p \widetilde{h}_r^* \right) \mathrm{d}\mu \mathrm{d}\lambda, \tag{23}$$

where $\mu = \sin(\varphi)$ and the asterisk $*$ denotes the complex conjugate. Subscript p refers to a particular mode corresponding to a zonal wavenumber k_p and a meridional index n_p. Subscript r indicates another mode.

GMDD
7, 8805–8873, 2014

Then, the linear operator (20) has the following property:

$$\langle \boldsymbol{W}_p, \mathbf{L}\boldsymbol{W}_r^* \rangle + \langle \mathbf{L}\boldsymbol{W}_p, \boldsymbol{W}_r^* \rangle = 0\,. \tag{24}$$

This can be verified by forming relevant inner products, integrating them globally, and using Green's theorem. For details see Platzman (1972).

By substituting Eq. (22) into Eq. (18) we find that $\boldsymbol{H}_p$ is the eigenfunction of $\mathbf{L}$ such that

$$\mathbf{L}\boldsymbol{H}_p = i\nu_p \boldsymbol{H}_p\,, \text{ and likewise } \mathbf{L}\boldsymbol{H}_r^* = -i\nu_r^* \boldsymbol{H}_r^*\,. \tag{25}$$

Therefore, by using Eqs. (22) and (25) we get from Eq. (24) that

$$\left(\nu_p - \nu_r^*\right) \langle \boldsymbol{H}_p, \boldsymbol{H}_r^* \rangle = 0\,. \tag{26}$$

Now we discuss very important properties of the eigenvalues and eigenfuctions of Eq. (20). Let us consider the following two cases of Eq. (26):
(1) The case of $p = r$. Because $\langle \boldsymbol{H}_p, \boldsymbol{H}_r^* \rangle$ becomes proportional to the total energy of the normal-mode solution of the linearized system that must not vanish, we require that $\nu_p = \nu_r^*$. Therefore, the ν_p must be real and we can drop the asterisk from the notation of eigenfrequency.
(2) The case of $p \neq r$. Because $\nu_p \neq \nu_r$, we must have $\langle \boldsymbol{H}_p, \boldsymbol{H}_r^* \rangle = 0$, meaning that $\boldsymbol{H}_p$ corresponding to ν_p must be orthogonal to the $\boldsymbol{H}_r$ associated with ν_r which is different from ν_p.

Since the magnitude of $\boldsymbol{H}_p$ is arbitrary, we use Eq. (23) to define the following normalization of $\boldsymbol{H}_r$:

$$\langle \boldsymbol{H}_p, \boldsymbol{H}_r^* \rangle = \delta_{pr}\,, \tag{27}$$

where the right-hand side is unity if $p = r$, and zero otherwise.

Separation of variables and the periodic boundary conditions in the longitudinal direction lead to the solution of $\boldsymbol{H}_n^k$ for discrete values of k in the form

$$\boldsymbol{H}_n^k(\lambda, \varphi) = \boldsymbol{\Theta}_n^k(\varphi) e^{ik\lambda}\,, \tag{28}$$

GMDD
7, 8805–8873, 2014

where the meridional dependence is described by the vector function $\mathbf{\Theta}_n^k$,

$$\mathbf{\Theta}_n^k(\varphi) = \begin{vmatrix} U_n^k(\varphi) \\ -iV_n^k(\varphi) \\ Z_n^k(\varphi) \end{vmatrix}, \tag{29}$$

which has three components: zonal velocity U, meridional velocity V, and geopotential height Z, all having zonal wavenumber k and meridional index n. The factor i, ($i = \sqrt{-1}$) in front of V is introduced to account for the phase shift of $\pi/2$ of V with respect to U and Z.

By substituting Eq. (28) with Eq. (29) into Eq. (27), we find

$$\int_{-1}^{1} \mathbf{\Theta}_p \cdot \mathbf{\Theta}_r^* \mathrm{d}\mu = \int_{-1}^{1} \left(U_p U_r + V_p V_r + Z_p Z_r\right) \mathrm{d}\mu = \delta_{pr}\,. \tag{30}$$

This is the orthogonality condition for Θ_p associated with frequency ν_p.

Various aspects of the eigensolutions of HSEs, including the methods of solution, their asymptotic characters, and tables of their eigenvalues (wave frequencies) and the eigenfunctions (meridional profiles) are discussed by Margules (1892), Hough (1898), Dikii (1965), Flattery (1967), Longuet-Higgins (1968), Kasahara (1976) and Phillips (1990). Because Hough (1898) was the first to solve the normal mode problem by means of spherical harmonics, the eigensolutions $\boldsymbol{H}_n^k$ as defined by Eq. (28) are now referred to as Hough functions (Siebert, 1961) or Hough harmonics.

There are three distinct manifolds of variability as the eigensolutions of the operator **L**. These are separated into two kinds of Hough functions: high-frequency westward and eastward propagating inertio-gravity waves (the so-called first kind solutions) and low-frequency westward propagating predominantly rotational waves of Rossby-Haurwitz type (the so-called second kind solutions). We denote the two kinds of solutions IG and ROT for inertio-gravity and Rossby–Haurwitz type of motions, respectively. For the zonal wavenumber $k = 0$ the second-kind of waves are degenerate. This

GMDD
7, 8805–8873, 2014

creates a difficulty in representing the zonally-averaged circulations. However, it is possible to derive the set of orthogonal functions for those modes as discussed by Kasahara (1978) and Shigehisa (1983). The software package that calculates the wave frequencies and associated Hough functions including their meridional derivatives by specifying the equivalent height and wavenumber was developed by Swarztrauber and Kasahara (1985) and it is a part of the present NMF software package.

Figure 1 shows the frequency behavior of the two classes of solutions for four equivalent depths: 10, 1 km, 100, and 10 m. Eastward-propagating solutions are shown for positive wavenumbers whereas negative wavenumbers correspond to the westward-propagating waves. Discrete values of frequencies are shown by symbols for the range of integer value of the zonal wavenumber from zero to 30. Frequencies for eastward propagating inertio-gravity and westward propagating inertio-gravity waves (EIG and WIG, respectively) are shown for the same range of zonal wave numbers. The lowest meridional mode of EIG solutions, $n = 0$ EIG, and balanced solutions, $n = 0$ ROT, are known as the Kelvin wave and the mixed Rossby-gravity wave and their properties have been investigated by Matsuno (1966) for the equatorial-β plane. Frequencies of the mixed Rossby-gravity (MRG) and the Kelvin wave (KW) fill a part of the frequency gap between the IG and balanced modes (other than MRG). For $D = 10$ km, a frequency gap between the IG and ROT waves is largest. As the equivalent depth reduces, the frequency gap becomes smaller while the frequencies of MRG and KW modes become more distinct from other frequencies. In particular, the frequencies of MRG waves at large scales become closer to that of WIG modes than to other ROT modes. In contrary, frequencies of KW at large scales become more separated from other EIG modes. Indeed, the observed properties of both MRG and KW in the tropical atmosphere had been associated with small equivalent depths of the order of 10 m (e.g. Wheeler and Kiladis, 1999).

Properties of equatorial MRG and Kelvin waves as well as of other eigensolutions of linearized shallow-water equations on the equatorial-β plane have been usually discussed with respect to the basic state of rest. The same applies to HSE (18) i.e. fre-

GMDD
7, 8805–8873, 2014

quencies of wave solutions associated with Eq. (18) and shown in Fig. 1 for several mean fluid depths do not include the effect of zonal flows. When the mean zonal flow is taken into account, frequencies of wave solutions of the linearized global shallow-water equations change (Kasahara, 1980). Kasahara (1980) showed that the frequency spectrum becomes in this case continuous (except for a few lowest ROT modes). Furthermore, solutions to such system can be unstable due to barotropic instability and as such they are not suitable for the representation of phenomena in global 3-D datasets. On the other hand, the structure of associated Hough functions does not change significantly when the basic state is not at rest (see Corrigendum to Kasahara, 1981). This implies that the application of the NMF software, which represent instantaneous atmospheric states in terms of Hough functions and vertical structure functions is not affected by the linearization around the state of rest.

2.4 Expansion of discrete global data onto NMF

An input data vector $\boldsymbol{X}$ for the projection is built by the zonal and meridional winds (u, v) and modified geopotential height $h = P/g$ defined on the horizontal regular Gaussian grid and vertical sigma levels at time step t, with the time subscript dropped.

$$\boldsymbol{X}(\lambda, \varphi, \sigma) = (u, v, h)^{\mathrm{T}}. \tag{31}$$

Equation (2) is applied to compute geopotential P.

The projection is performed on the precomputed vertical structure functions $G(\sigma)$, the meridionally dependent part of the horizontal Hough vector functions $\boldsymbol{\Theta}_n^k(\varphi)$ and harmonic waves in the longitudinal direction. The procedure derived in the previous section is applied in the steps summarized as follows. The input data on jth σ level are first represented by a series of the vertical structure functions $G_m(j)$. For a single data point $(\lambda, \varphi, \sigma_j)$ the expansion is

$$\begin{vmatrix} u(\lambda, \varphi, \sigma_j) \\ v(\lambda, \varphi, \sigma_j) \\ h(\lambda, \varphi, \sigma_j) \end{vmatrix} = \sum_{m=1}^{M} \mathbf{S}_m \boldsymbol{X}_m(\lambda, \varphi) G_m(j). \tag{32}$$

GMDD
7, 8805–8873, 2014

The scaling matrix $\mathbf{S}_m$ in Eq. (32), which makes the vector $\boldsymbol{X}_m(\lambda,\varphi)$ for the input to the horizontal structure equation dimensionless, is defined in accordance with Eq. (17) as

$$\begin{bmatrix} \sqrt{gD_m} & 0 & 0 \\ 0 & \sqrt{gD_m} & 0 \\ 0 & 0 & D_m \end{bmatrix}$$

The integer subscript m spans from the external vertical mode $m = 1$ to the total number of vertical modes M. Discrete functions $G_m(j)$ are derived using the finite difference solution method for the σ vertical coordinate in KP1981 and they satisfy

$$\sum_{j=1}^{J} G_m(j) G_{m'}(j) = \delta_{mm'} \,. \tag{33}$$

Here, J is the number of vertical levels. The vector $\boldsymbol{X}_m$ is calculated by the reverse transform of Eq. (32) through the multiplication of Eq. (32) by $G_{m'}(j)$ and summation of the result from $j = 1$ to J with the use of the orthogonality condition (33). The result becomes

$$\boldsymbol{X}_m(\lambda,\varphi) = \left(\widetilde{u}_m, \widetilde{v}_m, \widetilde{h}_m\right)^{\mathrm{T}} = \mathbf{S}_m^{-1} \sum_{j=1}^{J} (u,v,h)_j{}^{\mathrm{T}} G_m(j) \quad . \tag{34}$$

Definition of the vector $\boldsymbol{X}_m$ in Eq. (34) makes use of the notation defined in Eq. (17). Equations (32) and (34) are the vertical transform pair.

The dimensionless horizontal coefficient vector $\boldsymbol{X}_m(\lambda,\varphi)$ for a given vertical mode m can now be projected onto the Hough harmonics $\boldsymbol{H}_n^k$ as

$$\boldsymbol{X}_m(\lambda,\varphi) = \sum_{n=1}^{R} \sum_{k=-K}^{K} \chi_n^k(m) \boldsymbol{H}_n^k(\lambda,\varphi;m) \,, \tag{35}$$

GMDD
7, 8805–8873, 2014

where the maximal number of zonal waves is denoted by K, including zero for the mean zonal state. For every given vertical mode m, the Hough harmonics are characterized by the two indices for the combined meridional mode n and the zonal wavenumber k. The subscript n for the meridional mode indicates all combined meridional normal modes including N_R rotational (ROT), N_E eastward and N_W westward propagating inertio-gravity modes. Thus $R = N_R + N_E + N_W$. The global orthogonality condition for the Hough functions is Eq. (27).

The scalar complex coefficient $\chi_n^k(m)$ can be obtained from Eq. (35) by multiplying Eq. (35) by $\left[\boldsymbol{H}_n^k\right]^*$, the complex conjugate of $\boldsymbol{H}_n^k$, and integrating the resultant equation with respect to λ from 0 to 2π , and with respect to φ from $-\pi/2$ to $+\pi/2$, and using the orthonormality condition (27) . The result is

$$\chi_n^k(m) = \frac{1}{2\pi} \int_0^{2\pi} \int_{-1}^{1} \boldsymbol{X}_m(\lambda, \varphi) \cdot \left[\boldsymbol{H}_n^k\right]^* \mathrm{d}\mu \mathrm{d}\lambda \,. \tag{36}$$

Equations (35) and (36) are the horizontal transform pair.

2.5 Energy product

One of the advantages of expanding the fields of atmospheric motions by the normal mode functions is that the global total energy can be derived from a particular type of scalar product, called the energy product. A history on the origin of the energy product is discussed by Platzman (1992). Here, the energy product is calculated from the complex coefficients obtained by Eq. (36). The partition of total energy into the kinetic and available potential energies becomes straightforward. Likewise, the energy spectrum with respect to longitudinal, meridional and vertical scales as well as wave species can be calculated easily. A detailed derivation of global energy equation in the normal mode space from the linearized atmospheric model represented by Eqs. (3)–(5) has been presented in KP1981.

GMDD
7, 8805–8873, 2014

The conservation equation of global total energy in the system in the modal space is given by

$$\frac{\partial}{\partial t}\int_0^{2\pi}\int_{-1}^{1}\sum_{m=1}^{M}(K_m+P_m)\,\mathrm{d}\mu\mathrm{d}\lambda=0\,, \tag{37}$$

where

$$K_m=\frac{1}{2}\left(u_m^2+v_m^2\right) \tag{38}$$

and

$$P_m=\frac{1}{2}\frac{g}{D_m}h_m^2\,. \tag{39}$$

Here, K_m and P_m denote the specific kinetic energy and potential energy, respectively, of the mth vertical mode. The energy P_m may be more appropriately referred to as available potential energy which represents the available portion of the sum of the potential and internal energies of wave motions (Lorenz, 1955). From Eq. (34) it is clear that the components u_m, v_m and h_m are defined as

$$(u_m,v_m,h_m)^{\mathrm{T}}=\sum_{j=1}^{J}(u,v,h)_j{}^{\mathrm{T}}G_m(j)\quad. \tag{40}$$

The global energy product of the mth vertical mode is defined by the following scalar product I_m,

$$I_m=\frac{1}{2}gD_m\sum_{n=1}^{R}\sum_{k=-K}^{K}\chi_n^k(m)\left[\chi_n^k(m)\right]^*, \tag{41}$$

GMDD
7, 8805–8873, 2014

where $\left[\chi_n^k\right]^*$ is the complex conjugate form of Eq. (36) and it is given by

$$\left[\chi_{n'}^{k'}(m)\right]^* = \frac{1}{2\pi}\int_0^{2\pi}\int_{-1}^{1} \boldsymbol{X}_m(\lambda,\phi)\cdot\boldsymbol{H}_{n'}^{k'}\mathrm{d}\mu\mathrm{d}\lambda\,. \tag{42}$$

Note that in Eq. (41) the energy product is summed up with respect to the meridional mode index from $n = 1$ to R and zonal wavenumber $k = -K$ to K as done in Eq. (35).

Applying expression for $\boldsymbol{X}_m(\lambda,\phi)$ from Eq. (34) and orthogonality condition

$$\sum_{n=1}^{R}\sum_{k=-K}^{K}\frac{1}{2\pi}\int_0^{2\pi}\int_{-1}^{1}\boldsymbol{H}_n^k\cdot\left[\boldsymbol{H}_{n'}^{k'}\right]^*\mathrm{d}\mu\mathrm{d}\lambda = \delta_{kk'}\delta_{nn'}\,. \tag{43}$$

the scalar product I_m defined by Eq. (41) becomes

$$I_m = \frac{1}{2}gD_m\int_0^{2\pi}\int_{-1}^{1}\left(\widetilde{u}_m^2+\widetilde{v}_m^2+\widetilde{h}_m^2\right)\mathrm{d}\lambda\mathrm{d}\mu \tag{44}$$

$$= \int_0^{2\pi}\int_{-1}^{1}(K_m+P_m)\,\mathrm{d}\mu\mathrm{d}\lambda\,. \tag{45}$$

Thus, to obtain the global total energy I the summation of scalar product I_m with respect to the vertical mode is required as

$$I = \frac{1}{2}\sum_{m=1}^{M}gD_m\sum_{n=1}^{R}\sum_{k=-K}^{K}\left(\mathrm{Re}\left[\chi_n^k\right]^2+\mathrm{Im}\left[\chi_n^k\right]^2\right)\,. \tag{46}$$

GMDD
7, 8805–8873, 2014

Also note that similar to Eq. (41) we can express the global energy of the kth zonal wavenumber as I_k,

$$I_k = \frac{1}{2} \sum_{m=1}^{M} gD_m \sum_{n=1}^{R} \chi_n^k(m) \left[\chi_n^k(m)\right]^*, \tag{47}$$

and the global energy contained in the nth meridional mode as I_n,

$$I_n = \frac{1}{2} \sum_{m=1}^{M} gD_m \sum_{k=-K}^{K} \chi_n^k(m) \left[\chi_n^k(m)\right]^*. \tag{48}$$

3 Formulation of the NMF software

The software consists of a new code written mainly in Fortran 90 which needs to be applied together with several basic libraries available in the public domain. The external libraries needed for the software implementation are the libraries for handling the input data in GRIB and NETCDF formats and the LAPACK and ALFPACK libraries for solving the eigenvalue problem. While a version of the LAPACK (version 3.4) and a somewhat modified ALFPACK source code are provided with the package, the NETCDF and GRIB-API libraries need to be installed by the user. The ALFPACK package, which is used for the computation of the associated Legendre functions of the first kind, originates from NCAR (Swarztrauber and Kasahara, 1985).

Once the above libraries are correctly installed and their paths provided in *Mkinclude* file located in the main directory *NMF_MODES*, the execution of *make* command produces five binaries which compute

- the Gaussian grid and weights
- the vertical structure functions

GMDD
7, 8805–8873, 2014

– the horizontal structure functions

– projection of 3-D global data and

– filtering of selected modes back to physical space.

The first three executables need to be applied at the beginning of any project work related to a particular global dataset as they provide a set of eigenmodes for the projection. The main job, that of the 3-D projection, can be carried out for any number of input files which are recognized by their date flags. The same approach is applied in the case of modal filtering which reads an input file with the Hough coefficients $\chi_n^k(m)$ and provides their physical space equivalent for a user-defined subset of values (k, n, m).

All auxiliary input files are direct access binary files except the input file with the vertical coordinate definition which is kept in text format. Such files for the ECMWF system are available online, for example from http://old.ecmwf.int/products/data/technical/model_levels (as on 9 August 2014) and can be directly copied to the input file. All outputs files, vertical structure functions, horizontal structure functions, and output files of 3-D projection with the Hough expansion coefficients have the direct-access binary format. Outputs of the filtering can, in addition to direct-access binary format, be saved as text files. It is planned in future work to replace the binary format with the netcdf format for all input and output files.

Compilation is straightforward and it has been successfully applied on Linux systems and Mac OS as well as the large IBM and CRAY computers of ECMWF. The applied Fortran compiler is by default *gfortran*. Other compilers, the *Intel* Fortran and the IBM fortran have also been used and no problems specific to different compilers were found. The small and big endian computers have also been used.

3.1 Computation of the Gaussian grid parameters

The computation of the Gaussian grid on which the 3-D normal-mode projection is carried out is easily performed by specifying only two input values in the namelist

GMDD
7, 8805–8873, 2014

&gaussian in the input file name *gauss.cnf*. These are the number of the Gaussian grid points between the poles and the output file name which contains locations of the Gaussian points and their weights. An example is available in Appendix A. The subsequent computations of the meridional profiles of Hough functions, the projection and the modal filtering use this file. Input data for the projection thus need to be provided on the same regular Gaussian grid as the software performs no horizontal data interpolation. The regular Gaussian grid format is available for extraction directly from the ECMWF data archiving system MARS. Datasets from other centres such as other reanalyses and climate model outputs should be transformed to the Gaussian grid by the user. This can be done for example by using standard operators such as NCO (http://nco.sourceforge.net) and CDO (https://code.zmaw.de/projects/cdo).

3.2 Computation of the vertical structure functions

The described procedure for the NMF representation assumes that the input data are defined on the vertical σ levels or that they can be vertically interpolated to the predefined σ levels. If input data are not on σ levels, the definition of the σ coordinate needs to be provided. It is used as input to the vertical structure equation (10) and later on as input information for the interpolation from the levels of input data to σ levels. The software currently manages input data on σ and on hybrid levels and the latter are interpolated to the predefined sigma levels by the software. If the vertical coordinate is not sigma nor the hybrid sigma-pressure, there is no option available in the software but a user needs to define a σ coordinate for his/her input data. For example, the sigma coordinate for the standard-pressure level data can easily be computed as $\sigma = p/p_s$ and the vertical interpolation of input data needs to be performed from pressure to σ levels. As the software so far has mainly been applied to the ECMWF system data, which are defined on the hybrid vertical levels, subroutines for their interpolation to corresponding σ levels are well tested and included in the software.

In addition to the values of σ coordinate, the stability profile defined by Eq. (8) is another input to the program for the computation of the vertical structure functions. For

GMDD
7, 8805–8873, 2014

the hybrid coordinate of the ECMWF model and several climate models (e.g. NCAR climate model, EC-Earth) values of σ are readily obtained from the available values of average full and half-level pressures. In order to compute the stability profile, globally averaged temperature T_0 on σ levels needs to be specified. The profile of T_0 presented in Fig. 2a is computed from ERA Interim reanalyses for the year of 2000 but it varies little if a multi-year period is used instead. The same applies for stability profile computed by Eq. (8) from $\mathrm{d}T_0/\mathrm{d}\sigma$ and the σ levels. The profile of Γ_0 for ERA Interim is presented in Fig. 2b. It can be seen that the values of Γ_0 are positive and they vary little throughout the troposphere; however, in the upper stratosphere and the mesosphere Γ_0 increases a lot so that overall it can vary several orders of magnitude between the surface and 0.1 hPa. As a result, the stability parameter S which is computed for use in Eq. (10) has a profile with values rapidly increasing in the upper stratosphere (Fig. 2c).

Appendix B shows parameters of the input namelist *vsfcalc_cnf* in input file *vsfcalc.cnf* needed for the computation of vertical structure functions. In addition to the two binary input files, a user specifies the names of two outputs files containing the vertical structure functions and equivalent depths. In principle the number of vertical modes, which correspond to the number of vertical structure functions saved in the output file, is the same as the number of vertical sigma levels. However, one may not want to use all vertical structure functions in the projection due to small equivalent depths associated with higher vertical modes. As seen in Fig. 3 showing vertical structure functions for ERA Interim, equivalent depths have values ranging from about 10 km up to about cm or even a millimeter. There is a rapid drop in values of equivalent depth after the leading five vertical modes. In the case of ERA Interim presented in Fig. 3, there are four equivalent depths greater than 1 km, 11 equivalent depths between 1 km and 100 m while further 18 equivalent depths have values greater than 10 m. Between 10 and 1 m there are 14 depths and the remaining 13 values of equivalent depth are between 1 m and 4 mm. These values represent a separation constant coupling the vertical and horizontal structure equations. As illustrated in the next section, the meridional extent of the horizontal structure functions is associated with the magnitude of

GMDD
7, 8805–8873, 2014

D. The Hough functions corresponding to equivalent depths of the order of 10 m are meridionally bounded to the tropics.

Correspondingly, small equivalent depths have been extensively used to characterize various equatorial waves. This relies on the theory of tropical wave solutions derived for the equatorial-β plane (Matsuno, 1966). Instead of the Hough functions characterizing the spherical wave solutions, linear wave solutions for the shallow-water equations on the equatorial-β plane with the prescribed value of D are given in terms of the parabolic cylinder functions. The linear theory of tropical waves has been successfully employed to represent some of the most dominant variability of the tropical atmosphere (e.g. Gill, 1980; Heckley and Gill, 1984; Biello and Majda, 2005). The spectral-time filtering of tropical data has been used to derive the shallow-water phase speeds of equatorial waves coupled to convection; the estimated range of equivalent depths varies between 10 to 100 m (e.g. Hayashi, 1981; Wheeler and Kiladis, 1999).

As discussed in previous papers, the equivalent depth for the first vertical mode (m = 1) depends only on the surface temperature, which is a global constant, and the model vertical depth (Cohn and Dee, 1989). The equivalent depths for $m > 1$ are relatively insensitive to the value of the surface boundary condition, but they are sensitive to the stability and the depth of the top model layers (Staniforth et al., 1985). In the case of ERA Interim, there are on average 12 levels beneath 850 hPa, 10 levels from 850 to 500 hPa, 13 levels between 500 and 100 hPa whereas remaining 25 levels are in the stratosphere (21 levels under 1 hPa) and mesosphere (4 levels above 1 hPa). If instead of 60 hybrid models levels we select only 21 levels closest to the standard pressure levels, the corresponding equivalent depths are different for higher vertical modes as can be seen in Fig. 3b.

The shapes of vertical structure functions for the ERA Interim 60-level system are shown in Fig. 4a and b for the first seven vertical modes (Fig. 4a) and for selected higher modes (Fig. 4b). The solutions for first seven vertical modes are shown also for the case of 21 levels (Fig. 4c) defined by values of average pressure closest to the standard pressure. This figure can be compared with other figures from literature

GMDD
7, 8805–8873, 2014

including plots from KP1981 and Žagar et al. (2009a). Each vertical mode m is associated with $m-1$ zero crossings in the vertical profile. Therefore the mode $m=1$, which does not change sign, has traditionally been referred to as the barotropic mode. Lower modes have larger amplitudes in the troposphere and the stratosphere, whereas the relevant structure of G_m functions moves downward towards the surface as the value of m increases (Fig. 4b). We can note that the second mode has its single zero crossing at around 30 hPa and that the leading seven modes have no zero crossings under 300 hPa. Traditionally these modes have been referred as the first baroclinic mode, the second baroclinic mode and so on in the discussion of tropospheric circulation. However, such terms are not suitable in the present case of models with model top levels high above the tropopause. Since several vertical modes correspond to the traditional picture of the first baroclinic mode, using any one of them provides an incomplete picture of the circulation associated with the "first baroclinic mode". Instead, we need to sum up a number of vertical modes in order to discuss representative circulation in physical space.

3.3 Computation of the horizontal structure functions

A separate program for the computation of the horizontal structure functions computes the meridional structure of Hough harmonics, i.e. vectors $\boldsymbol{U}_n^k(\phi)$, $\boldsymbol{V}_n^k(\phi)$ and $\boldsymbol{Z}_n^k(\phi)$ for a range of values k and n for each equivalent depth. Appendix C shows parameters which need to be specified in the input file *houghcalc.cnf* through several namelists. Two input namelists, *meridional_grid* and *vsf_cnf* are known from earlier. In the namelist *vsf_cnf*, the user specifies the number of vertical modes (i.e. equivalent depths) for which the horizontal structure functions are computed. The range of horizontal modal indices is specified in *houghcalc_cnf* namelist by the initial (*szw*) and final (*ezw*) values of the zonal wavenumber and by the number of meridional modes (parameter *maxl*). Currently the same value of meridional modes *maxl* applies to all three motions types, EIG, WIG and ROT modes, so that the total number of meridional modes is $R = 3\times maxl$. The namelist *output* defines the name of the output files with Hough

GMDD
7, 8805–8873, 2014

meridional profiles and how the outputs are stored (binary or text format). Further explanations are provided in Appendix C.

The size of output binary files can be relatively large if a large zonal and meridional truncation is requested. For example, for the presented ERA Interim dataset, we have used 200 zonal wavenumbers and 70 meridional modes for each of the inertio-gravity and balanced modes. With a single file per zonal wavenumber, there are as many files with meridional structure of Hough function as zonal wavenumbers. The computation of horizontal structure functions is also the most memory demanding computation. However, once these files are computed, they can be used repeatedly for the projection purposes and they are read only once at the beginning of projection and filtering.

The meridional profiles of the Hough functions corresponding to the Kelvin mode and to the $n = 1$ balanced mode are shown in Fig. 5 for two zonal wavenumbers and for two vertical modes. The displayed vertical modes $m = 1$ and $m = 10$ have equivalent depths about 10 km and 220 m, respectively. We can see that an increased value of vertical modes, i.e. a reduced value of equivalent depth is associated with a stronger equatorial trapping of the horizontal structure functions. Similar equatorial trapping of horizontal structure functions occurs when the zonal wavenumber increases for the same equivalent depth. In Fig. 5 the solution for $(k, m) = (1, 10)$ appears equatorially trapped nearly as much as the solution for $(k, m) = (31, 1)$. For the barotropic mode, the horizontal structure of all modes is global. This tells us that numerically obtained small equivalent depths associated with vertical structure function that are representative only for the lower troposphere and the boundary layer are not useful for the projection of data in the extra-tropical regions. Therefore, even if one can solve the vertical structure equation for all vertical modes, the number of vertical modes we keep in the computation of the horizontal structure functions (parameter *num_vmode* in namelist *vsf_cnf* in Appendix C) should in principle be quite smaller than the number of model levels. For the results presented in the next section for ERA Interim, we kept 43 vertical modes with equivalent depths greater than 1 m. While it is not wrong to keep all vertical modes, we

GMDD
7, 8805–8873, 2014

found that not using vertical modes with equivalent depth smaller then 1 m is a good option in the case of models with many vertical levels such as the ECMWF model.

3.4 Projection of 3-D data on normal-mode functions

Namelists for the meridional grid and vertical structure functions defined in previous subsections are used also in the input file *normal.cnf* for the projection that is given in Appendix D. In addition, namelist *hough_cnf* specifies input files with the meridional Hough functions while the remaining namelists provide information about the input data. The user can choose to save the globally averaged vertical temperature profile T_0 and surface pressure field. These can be used for a posteriori interpolation from sigma levels back to the hybrid (or other) model levels or for the computation of temperature perturbations from the geopotential perturbations. Namelist *input_data* describes the data format and the vertical grid. The data valid for a single time step can be contained in several files which together must contain fields of temperature, wind components and specific humidity on model levels as well as surface pressure and orography. Horizontally all fields must be on the regular Gaussian grid. Specific humidity is used in the computation of model-level geopotential and if not available it could be neglected; i.e. temperature instead of virtual temperature can be used for the computation of geopotential height (note that this option is not available yet in the software).

The projection software works in the following way. First the input files with the meridional grid, vertical structure functions and horizontal structure functions are read. This is followed by the input data reading. The modified geopotential variable is computed on the input model levels that are afterward interpolated vertically to the predefined sigma levels if needed. This provides the input vector $\boldsymbol{X}$ defined by Eq. (31). The vertical projection (34) is carried out first followed by the horizontal projection (36). The resulting Hough coefficients are saved in the output file with name prefix defined by the variable *coef3-DNMF_fname* which is appended by the date as specified in the namelist *time*. (Currently the output file is a direct-access binary file but in future we plan to make it a netcdf format file.) The data reading and the projection step are carried in the loop

GMDD
7, 8805–8873, 2014

over time which is defined in the namelist *time*. Variable *dt* defines a regular time step between subsequent files. Outputs of the projection of 30 year ERA Interim data (once per day at 12:00 UTC) are presented in the next section.

3.5 Filtering of modes to physical space

The inverse projection or filtering of modes back to physical space is defined by Eqs. (35) and (32) for the inverse horizontal and vertical projections, respectively. Not all modes need to be inverted back to physical space. For example, it may be of interest to separate the balanced and IG components of circulation. Tropical modes are of special interest as many studies deal with the characteristics of the Kelvin mode and mixed Rossby-gravity mode throughout the tropical atmosphere. The NMF software allows to filter any mode or a set of modes back to physical space.

Appendix E contains an example of input file *normal_inverse.cnf* for the filtering of selected range of (k, n, m) modal indices. In addition to several namelists shared with the file *normal.cnf*, two namelists, *normal_cnf_inverse* and *filter_cnf* are needed specifically for the filtering purpose. The former is similar to *normal_cnf* as it defines the input and output file names and formats. The latter defines the range of the zonal, meridional and vertical modes which are to be filtered out. The meridional filtering range is defined separately for the EIG, WIG and balanced modes. If the filtering range is specified in terms of the zonal wavenumbers or vertical modes, the range of associated meridional modes to be filtered out can be specified by the user. No filtering out of any modes can be achieved simply by choosing the index value of the starting mode to filter (e.g. *eig_n_s*) greater than the truncation value for the same mode (i.e. *eig_n_s* > *maxl*). In the next section we shall discuss outputs of filtering of the balanced and IG circulation.

GMDD
7, 8805–8873, 2014

4 Modal analysis of ERA Interim: climatological properties

Now we present some average properties of the 30 year (period 1980–2009) reanalysis data from ERA Interim (Dee et al., 2011). Fields available on 512 × 256×60 grid every day at 12:00 UTC during 30 years were projected using namelist parameters provided in Appendix D. This provides about 11 000 output files with $\chi_n^k(m)$ coefficients to be analyzed statistically. The presented averages are obtained in various ways. The global energy distribution presented in Figs. 6–8 is obtained by averaging energy in a single zonal wavenumber and meridional mode as defined by Eqs. (47) and (48), respectively. Zonal averages, cross-equatorial flow and horizontal circulation on selected levels are produced by averaging coefficients $\chi_n^k(m)$ over 30 years for each mode followed by the inverse projection to physical space based on filtering criteria. Appendix E provides an example of namelist for filtering IG circulation.

4.1 Scale-dependent energy distribution

In Fig. 6 we first present average energy distribution as a function of the zonal wavenumber as defined by Eq. (47). The spectra are shown up to the maximal truncation used for the projection, zonal wavenumber 200, which corresponds to a grid spacing about 100 km at the equator and about 70 km in midlatitudes. One can see that the total energy spectra follow well the −3 law all the way from the synoptic scales ($k > 5$) down to the the smallest analyzed scale. As in Žagar et al. (2009a) we note a major difference between the balanced and unbalanced energy spectra; the latter are characterized by a more flat slope, especially on planetary and synoptic scales. Furthermore, IG energy is not equally split into EIG and WIG contributions, as shown in Fig. 6b. On planetary scales, EIG dominate and this is largely a contribution of the Kelvin waves as noted in the previous study (Žagar et al., 2009b).

For the planetary wave numbers 1–5 the total (and balanced) energy spectrum is more flat than for synoptic scales; energy injected at scales associated with baroclinic instability inversely cascades to larger scales (Charney, 1971). The energy scaling law

GMDD
7, 8805–8873, 2014

in planetary scales appear closer to −1 than to theoretically expected −5/3 law (e.g. Lilly, 1973). Further details about this part of the spectrum can be discussed in relation to Fig. 6c which shows balanced energy spectra for different meridional modes. The MRG spectrum (denoted $n = 0$ ROT) appears flat at planetary scales, a feature noticed also in operational ECMWF analyses by Žagar et al. (2009b). Balanced energy spectra for meridional modes 1–5 which represent majority of variability in midlatitudes have a −5/3 slope as expected by the quasi-geostrophic turbulence theory (Charney, 1971; Tung and Orlando, 2003).

The total energy distribution shows no sign of slope flattening in subsynoptic scales in comparison to synoptic scales. On the contrary, after zonal wavenumber around 100 the total energy spectrum becomes somewhat more steep (Fig. 6a). This lack of variability in subsynoptic scales has been noted also in other studies of numerical weather prediction models (e.g. Frehlich and Sharman, 2008) including the NMF results of various analysis systems (Žagar et al., 2009a). One can also notice in Fig. 6a that the slope of IG energy spectra becomes steeper as the horizontal scale reduces. In subsynoptic scales, IG energy clearly dominates over balanced energy.

A relative contribution of the two energy components is further presented in Fig. 7. This figure shows that at the zonal wavenumbers 28–30, which correspond to the resolution of about 700 km at the equator and to around 500 km in the midlatitudes, the unbalanced component of energy becomes greater than the balanced component. Given the global 3-D nature of our spectra and a lack of previous similar investigations, it is difficult to discuss the origin of this scale in ERA Interim data and its realism. A similar scale has been known from observations as the scale of the major shift in the slope of energy spectra (derived for both wind and temperature data) from −3 to −5/3 range (Nastrom and Gage, 1985). However, a similar change of the slope of the total energy spectra is absent in Fig. 6. Furthermore, energy spectra derived from models are usually based on single level data (e.g. Burgess et al., 2013; Blažica et al., 2013) and they show only kinetic energy; correspondingly, their comparison with the spectrum in Fig. 6a which represents the vertically integrated total energy is not simple. Blažica

GMDD
7, 8805–8873, 2014

et al. (2013) showed that on mesoscale in midlatitudes the divergent component of kinetic energy is at least equally large as the rotational component and that the slopes of the corresponding spectra depend on the altitude (see also Burgess et al., 2013). In our global case with the tropics dominated by divergent circulation, we find that the unbalanced component makes 80 % or more of total energy beyond the zonal wavenumber 100 (about 150 km in midlatitudes) (Fig. 7). On the contrary, on planetary scales it is about 10 % of energy or less. However, as the large-scale energy dominates the overall contribution of unbalanced energy to total energy is somewhat less than 10 %. In planetary scales only (zonal wavenumbers 1–5) there is 80 % of total energy; synoptic scales (zonal wavenumbers 6 to 15) contain about 15 % of the global total energy while subsynoptic scales ($k > 15$) contribute about 5 % of the total global energy in ERA Interim. Since reanalyses such as ERA Interim provide the most reliable picture of general circulation, the number above can be used to evaluate energy distribution in climate models.

The meridional energy distribution is presented in Fig. 8. The dominance of balanced energy over IG energy is clearly seen for all meridional modes except for the lowest one, $n = 0$. The reason is that the lowest meridional mode for EIG modes is the Kelvin mode while the mixed Rossby-gravity wave is saved as $n = 0$ balanced mode. The Kelvin wave is the most energetic unbalanced mode of the global atmosphere (Žagar et al., 2009b) and its energy level, especially when shown together with $n = 0$ WIG mode, exceeds the energy level of the MRG mode. The balanced energy distribution has a peak in the meridional modes $n = 3$–7 which have the most significant structure in the midlatitudes (not shown). As n increases, the IG energy component reduces much more rapidly than the balanced energy component. This can be expected since as n increases, the meridional structure of mode becomes less and less relevant for the tropics where IG circulation dominates.

From the physical point of view it is more complicated to discuss the energy distribution as a function of the vertical mode. As discussed in the previous section, it is difficult to discuss a single vertical mode separately except perhaps the barotropic mode. Nev-

GMDD
7, 8805–8873, 2014

ertheless, the vertical energy distribution displays characteristics for the balanced and IG modes that can be physically interpreted. In particular, the vertical distribution of IG energy appears related to tropical convection which generate majority of tropical IG motions. Several distinct maxima in energy distribution can be associated with free propagating large-scale IG modes, with deep convection and with convectively-coupled waves (figure not shown). An exact physical interpretation of these energy maxima in relation to dominant equatorial waves derived from observations can be obtained by filtering these vertical modes back to the physical space and comparing their properties with independent observations. This is a subject of a separate paper.

4.2 Average circulation

Figure 9 shows the zonally averaged zonal wind in January and July, averaged over the ERA Interim period 1980–2009. Three figures for each month correspond to the total, balanced and IG component. The sum of the balanced and IG components correspond to the total average zonal wind. While Fig. 9a and d resemble the known properties of the zonally averaged zonal wind from earlier reanalyses and GCMs (e.g. Hartman, 2007), splitting of circulation in the balanced and IG components has not been presented earlier. Figure 9 shows that the IG component is nonzero in the polar regions of the Southern Hemisphere in both seasons and in the winter stratosphere. In January, there are easterlies in polar region south of 60° S up to about 300 hPa and westerlies above. In July, IG easterlies are found from the surface up to 500 hPa. There is a weak unbalanced component of the zonal wind near the surface in the tropics and in the upper stratosphere above 30 hPa in the winter hemisphere. Tropospheric unbalanced easterlies are associated with the impact of Antarctic orography on circulation which in model-level data projects onto IG modes as a stationary signal. In addition, the gradient wind balance must be a contributing factor to the strength of IG circulation in the winter stratosphere (polar vortex) and possibly also in the troposphere around Antarctica. Similarly, a non-zero zonally averaged meridional wind is found in the upper tropical troposphere and near the surface in the subtropical region in the winter hemisphere in

GMDD
7, 8805–8873, 2014

relation to the flow from the summer to the winter hemisphere (Fig. 10). Although the average meridional winds in the extra tropics are weak, notice their presence in the boundary layer of the Southern Hemisphere as well as in the summer tropical stratosphere. As the zonally-averaged meridional wind is completely associated with the IG circulation, the balanced and total components are not shown (figures appear identical).

A further insight about the meridional wind in the tropics is provided in Fig. 11 that shows its structure along the equator for balanced and IG parts. In this figure, several known dynamical properties of tropical circulation can be associated with the balanced and IG components. In January, we recognize vertically propagating IG waves in the stratosphere (Fig. 11a and c). The cross-equatorial flow in the upper troposphere and near the surface are in opposite directions and mostly associated with the IG modes. A shift from the northerly to the southerly winds from winter to summer associated with the movement of the Hadley cell and ITCZ is especially intense in the Indian ocean sector due to monsoon. Another feature seen in Fig. 11 is the impact of orography, well seen in the lower troposphere due to land massif of Africa and in the eastern Pacific due to the Andes. Such features of the lower tropospheric circulation are absent when the vertical structure of circulation is analyzed by using data on standard pressure levels which remove the impact of orography by the interpolation. While the presented complex structure of winds near the surface may appear less familiar, these are realistic winds as analyzed by ERA Interim on its hybrid model levels which are almost the same as sigma levels close to the surface. We do not go into more detailed research of various features in Figs. 9–11 as their proper study and more exact quantification of the IG component is beyond the scope of the present paper. Our purpose is primarily to illustrate the diagnostic capabilities of the NMF software.

The horizontal climatological structure of wind field is shown in several figures for two levels. We display model level 51 which is located in the lower troposphere close to 900 hPa and at model level 31 located at about 229 hPa as an example of the upper tropospheric flow. January and July circulation are compared in Figs. 12–15 for

GMDD
7, 8805–8873, 2014

the upper troposphere (Figs. 12 and 14) and the lower troposphere (Figs. 13 and 15). These figures show that the IG circulation, although just a part of the total wind, has an important role in providing a major part of the cross-equatorial flow. It modifies the large-scale balanced flow which is primarily zonal across most of the tropics except in the eastern Pacific. In January, the meridional component of unbalanced winds over western Pacific and Indian ocean is providing the cross-equatorial circulation by turning the balanced winds to the south-easterly directions (Fig. 12); the opposite applies in July when the IG component enhances cross-equatorial circulation by adding the northern component to balanced easterlies over Indonesia and Indian ocean (Fig. 14). A dominant feature of IG circulation in July is an almost purely divergent flow over the south-east Asian monsoon region. Another outflow region is found over South America.

The IG circulation close to 900 hPa is comparable in magnitude to the balanced flow. Climatological meridional winds in the central and western Pacific and Indian ocean in ERA Interim come mainly from the unbalanced flow, especially in January (Fig. 13). Thus the ITCZ location is defined by the IG circulation. The extent to which this result is associated with the model dynamics and physics i.e. the first-guess field in data assimilation in comparison to observations and the multivariate coupling imposed through the 4-D-Var in the ERA Interim system is a complex question beyond the scope of this paper.

Finally, we show an example from the climatology of the most studied mode of tropical dynamics, the Kelvin mode. In Fig. 16 the Kelvin wave is shown at two levels; besides the upper troposphere level 31 shown in other figures we also show model level 27 closer to the tropical tropopause, where the Kelvin amplitude is largest in July. The prevalent feature of Kelvin wave climatology is the zonal wavenumber $k = 1$ structure with a negative geopotential perturbation in the upper troposphere over the Indian ocean and equatorial Africa (easterlies) and a positive perturbation over the most of the Pacific (westerly winds). The lower troposphere has approximately an opposite picture over the Pacific with strongest easterlies over the western and central Pacific (not shown). The climatological Kelvin wave signal is very weak over Atlantic and South

GMDD
7, 8805–8873, 2014

America in the upper troposphere. This suggests that the climatological picture of the tropics as envisaged by Gill (1980) and implemented in many reduced models of the tropics (e.g. Majda et al., 2004) applies best to the western Pacific where the low-level easterlies in ERA Interim are due to the Kelvin wave response to the heating over Indonesia. A steady-state response from idealized models including the long-wave approximation, as is assumed in many theoretical studies, in other tropical basins than the western and central Pacific appears appreciably modified by other IG modes than the Kelvin wave and by the mixed Rossby-gravity mode, in agreement with expectations from more complex studies (e.g. Kasahara, 1984; Geisler and Stevens, 1982).

5 Conclusions

We presented the theory of the normal-mode functions, technical details of the code dealing with their application on global 3-D data and examples of the software application of the reanalysis dataset ERA Interim. It is argued and illustrated by examples that the normal mode procedure, once an important part of the initialization of NWP models, can be applied for a range of other topics. In particular, normal modes can be used to evaluate the unbalanced circulation across many scales. Current global observing system provides an unprecedented amount of observations, mainly from satellites which, together with advanced assimilation procedures and high resolution global models, for the first time in history allow one to resolve inertio-gravity waves across many scales (e.g. Shutts and Vosper, 2011). Furthermore, improved vertical discretization, raised model top level and complex parametrizations of moist processes have proven to successfully represent vertical wave propagation, especially in the tropics. Thus, operational analyses display significant similarities regarding the large-scale divergent modes (e.g. Žagar et al., 2009b). This is encouraging for the validation of climate models by using normal modes, an application envisaged early by Williamson and Dickinson (1976). Evaluation of present-day and past climates simulated by climate models by their comparison with analyses and newest reanalyses is crucial in

GMDD
7, 8805–8873, 2014

relation to climate scenarios. As the models are characterized by significant problems in simulating the tropical interseasonal variability (e.g. Lin et al., 2006) validation of the global unbalanced circulation can lead to new understanding of models' deficiencies and provide new ideas for their improvements.

In particular, spatio-temporal details of the large-scale equatorial modes such as the Kelvin wave are identified simultaneously in the mass field and wind field. Furthermore, the analysis is done by considering the whole model depth in contrary to majority of existing studies. Although the NMF representation is applied independently on instantaneous atmospheric states, the time series of Hough projection coefficients for various modes and their physical-space equivalents link together to provide a spatio-temporal picture consistent with the linear wave theory which has been the backbone of our understanding of atmospheric dynamics. This has been illustrated in Žagar et al. (2009b) whereas a long-term analysis of the vertical wave propagation in ERA Interim is under preparation. As such, the NMF method for wave identification is complementary to other methods such as the spectral-temporal filtering. An important advantage of the NMF method is information on the variance contained in each wave number and mode.

The paper has presented technical details of the software implementation which is considered user friendly. A limited knowledge of Fortran (or a similar programming language) is judged sufficient to implement and modify the software. The software application is controlled through a limited number of parameters in several namelists. A set of open-source libraries for reading the input data and for solving the eigenvalue problem are used as well as gfortran compiler for the software compilation.

The presented representation of ERA Interim dataset in terms of normal-mode functions has revealed climatological features of the large-scale circulation. We showed that the global energy distribution is dominated by the balanced energy with the IG modes making less than 10 % of the total wave energy. However, beyond the zonal wavenumber 30 (scale around 700 km) the level of global IG energy exceeds the level of balanced energy. Even though the presented energy distribution is not in agreement with observations as the slope of spectra remains −3 all the way to the smallest resolvable

GMDD
7, 8805–8873, 2014

scale, this result is as good as possible at this point to validate the energy distribution and balance in climate models. Similar reasoning applies to other presented features such as the zonally-averaged and equatorial circulation.

The software is available from http://www.fmf.uni-lj.si/~zagarn/modes.php and support to its implementation is provided by the MODES team at the University of Ljubljana. The real time spectra and maps of the balanced and inertio-gravity circulation in the operational ECMWF forecast model can be found at http://meteo.fmf.uni-lj.si/MODES

Appendix A: Input file gauss.cnf for the definition of the regular Gaussian grid

```
& gaussian
  N = 256,
  gauss_fname = “gauss256.data”,
  /
  N – number of points between the poles
  gauss_fname – name of the output binary file with Gaussian points and weights
```

Appendix B: Input file vsfcalc.cnf for the definition of the vertical structure functions

```
& vsfcalc_cnf
  stab_fname = “stability_L60.data”,
  vgrid_fname = “sigma_levels_L60.data”,
  vsf_fname = “vsf_L60.data”,
  equiheight_fname = “equivalent_height_L60.data”,
  num_vmode = 60,
  mp = 60,
  hstd = 8000.0d0,
  suft = 288.0d0,
```


GMDD
7, 8805–8873, 2014

given_stability = .true.,
given_vsf = .false.,
ocheck = .true.,
/

stab_fname – input file with values of stability Γ_0 on sigma levels
vgrid_fname – input file with value of full sigma levels
vsf_fname – output file with vertical structure functions
equiheight_fname – output file with equivalent depths
num_vmode – number of vertical modes for which structure functions are stored in the output file
mp – number of grid points of the input vertical grid
hstd – scale height
suft – global surface temperature
given_stability – logical switch if the file with vertical structure functions is provided
ocheck – logical switch if the orthogonality is checked for the vertical modes

Appendix C: Input file houghcalc.cnf for the definition of the horizontal structure functions

```
& houghcalc_cnf
  szw = 0,
  ezw = 200,
  maxl = 70,
  my = 256,
  freq_fname = "freq.data",
  ks_mode = "K",
  ocheck = .false.,
  /
& meridional_grid
```


GMDD
7, 8805–8873, 2014

```
  ygrid_fname = “gauss256.data”,
  /
& vsf_cnf
  equiheight_fname = “equivalent_height_L60.data”,
  num_vmode = 43,
  /
& output
  output_gmt = .false.,
  ofname_gmt = “hough_gmt”,
  ofname_bin = “hough”,
  bin_combine = “zonal”,
  /
```

szw – starting zonal wavenumber to compute meridional structure of Hough harmonics

ezw – last zonal wavenumber to compute meridional structure of Hough harmonics

maxl – total number of meridional modes for each motion type (e.i. EIG, WIG, ROT), so that meridional modes range from zero to maxl -1

freq_fname – name of the file with dimensionless frequency v_n^k

ks_mode – type of solution for the case of $k = 0$*. Although it can be either “K” or “S”, the recommended value is “K”*

ocheck – a logical variable which in case of being .true. provides the horizontal orthogonality check (Eq. 27)

equiheight_fname – input filename with values of equivalent depths

num_vmode is a number of vertical modes i.e. a range of equivalent depths for the computation of meridional Hough profiles

output_gmt – logical variable which allows to save Hough profiles also in text format

ofname_gmt – name of outputs file in text format

ofname_bin – name of the output binary file

bin_combine – method to combine output. Default is “zonal” which means that solu-

GMDD
7, 8805–8873, 2014

tions for all vertical and meridional modes for a single zonal wavenumber are combined in a single file

Appendix D: Input file normal.cnf for the projection of 3-D data to NMFs

```
& normal_cnf
   nx = 512,
   ny = 256,
   nz = 60,
   nstep = 1,
   coef3-DNMF_fname = “Hough_coeff_”,
   output_3-DNMF = .true.,
   saveps = .false.,
   savemeant = .false.,
   ps_fname = “Ps_”,
   meant_fname = “Tmean_”,
   saveasci = .false.,
   afname = “Inputa_”,
   aformat = “(512E20.4,1x)”,
   /
& time
   datetype = “yyyymmddhh”,
   syear = 1980,
   smon = 01,
   sday = 01,
   shour = 12,
   smins = 00,
   ssec = 00,
   slen = 00,
```


GMDD
7, 8805–8873, 2014

```
  eyear = 2009,
  emon = 12,
  eday = 31,
  ehour = 12,
  emins = 00,
  esec = 00,
  elen = 00,
  dt = 86 400,
  /
& input_data
  dataformat_input = “grib”,
  orig = “ECMWF”,
  zgrid_type = “hybrid”
  numoffile = 1,
  ifile_grib_head(1) = “erai_an_N128_”
  ifile_rib_head(2) = ”
  /
& hough_cnf
  hough_fname = “hough”,
  num_zw = 200,
  maxl = 70,
  my = 256,
  /
& meridional_grid
  ygrid_fname = “gauss256.data”,
  /
& vsf_cnf
  vsf_fname = “vsf_L60.data”,
  vgrid_fname = “sigma_levels_L60.data”,
```


GMDD
7, 8805–8873, 2014

```
  equiheight_fname = “equivalent_height_L60.data”,
  model_level_fname = “model_levels_L60.dat”,
  num_vmode = 43,
  zgrid = “Sigma”,
  mp = 60,
  top = 1.0,
  given_vsf = .true.,
  /
```

nx – number of data point in the zonal direction

ny – number of data point in the meridional direction

nz – number of data point in the vertical direction

output_3-DNMF – true if outputs of expansion are saved

coef3-DNMF_fname – prefix of the output files with Hough expansion coefficients. The date is added according to the format specified in namelist time

saveps – true if input surface pressure should be saved upon reading

ps_fname – prefix of the name of file with input surface pressure

savemeant – true if globally-averaged vertical temperature profile should be saved

meant_fname – prefix of the name of file with temperature profile

saveasci – true if input 3-D data on model levels should be saved upon reading in text format

afname – prefix of the name of file with input data

aformat – format for input 3-D data saving

datetype – format of the time flag of input data. “yyyymmddhh” stands for checking of the data year, month, day, hour and forecast length

syear, eyear – first and last data year to be analyzed

smon, emon – first and last data month to be analyzed

day, eday – first and last day to be analyzed in relation to their year and month

shour, smins, ssec, ehour, emins, esec – hours, minutes and seconds of the data

elen – forecast length. “00” for analyses

GMDD
7, 8805–8873, 2014

dt – time step of subsequent times to be analyzed (in seconds)
dataformat_input – format of the input data file
orig – originating data center
zgrid_type – vertical coordinate
numoffile – number of data files per time step
ifile_grib_head – prefix of the input data file. The rest if the file name if made of the date

Appendix E: Input file normal_inverse.cnf for modal filtering

```
& normal_cnf_inverse
  nx = 512,
  ny = 256,
  nz = 60,
  nstep = 1,
  coef3-DNMF_fname = “Hough_coeff_”,
  inverse_fname = “ Inverse_allmodes_”,
  inv2hybrid = .false.,
  ps_fname = “ Ps_”,
  meant_fname = “Tmean_”,
  saveasci = .true.,
  afname = “AInverse_allmodes_”,
  aformat = “(512E12.4,1x)”,
  /
& filter_cnf
  eig_n_s = 100,
  eig_n_e = 70,
  wig_n_s = 100,
  wig_n_e = 70,
```


GMDD
7, 8805–8873, 2014

```
  rot_n_s = 1,
  rot_n_e = 70,
  kmode_s = 300,
  kmode_e = 200,
  vmode_s = 301,
  vmode_e = 43,
  /
& time
  ...
  /
& hough_cnf
  ...
  /
& meridional_grid
  ...
  /
& vsf_cnf
  ...
  /
```

coef3-DNMF_fname – prefix of the input file name with Hough expansion coefficients to be inverted to physical space

inverse_fname – prefix of the output file name with zonal wind, meridional wind and modified geopotential on sigma levels in physical space

inv2hybrid – true if interpolation from sigma to hybrid model levels is performed upon filtering

to compute winds and geopotential on hybrid levels

ps_fname – prefix of the input file name of surface pressure file

meant_fname – prefix of the input name of file with temperature profile

saveasci – true if output of inverse should be saved also in text format

GMDD
7, 8805–8873, 2014

afname – prefix of the name of output text format
aformat – format for output 3-D data saving
eig_n_s, eig_n_e – first and last EIG mode to be filtered out.
For each mode filtered out, all zonal wavenumber and all vertical modes are taken into account
wig_n_s, wig_n_e – first and last WIG mode to be filtered out
rot_n_s, rot_n_e – first and last ROT mode to be filtered out
kmode_s, kmode_e – first and last zonal wavenumber to be filtered out.
For each zonal wavenumber filtered out, all meridional and vertical modes are taken into account
vmode_s, vmode_e – first and last vertical mode to be filtered out.
For each vertical mode filtered out, all meridional and zonal modes are taken into account

The Supplement related to this article is available online at doi:10.5194/gmdd-7-8805-2014-supplement.

Acknowledgements. Development of the NMF software as an open-access tool and its application is carried out under the funding from the European Research Council, Grant Agreement no. 280153. The National Center for Atmospheric Research is sponsored by the National Science Foundation. The authors would like to thank Patrick Callaghan for his comments on the manuscript.

References

Baer, F. and Tribbia, J.: On complete filtering of gravity modes through nonlinear initialization, Mon. Weather Rev., 105, 1536–1539, 1977. 8808
Biello, J. A. and Majda, A. J.: A new multi-scale model for the Madden–Julian Oscillation, J. Atmos. Sci., 62, 1694–1721, 2005. 8830
Blažica, V., Žagar, N., Strajnar, B., and Cedilnik, J.: Rotational and divergent kinetic energy in the mesoscale model ALADIN, Tellus A, 65, 18918, 2013. 8836

GMDD
7, 8805–8873, 2014

Boer, G. J. and Shepherd, T. G.: Large-scale two-dimensional turbulence in the atmosphere, J. Atmos. Sci., 40, 164–1184, 1983. 8807
Burgess, B. H., Erler, A. R., and Shepherd, T. G.: The troposphere-to-stratosphere transition in kinetic energy spectra and nonlinear spectral fluxes as seen in ECMWF analyses, J. Atmos. Sci., 70, 669–687, 2013. 8836, 8837
Chapman, S. and Lindzen, R. S.: Atmospheric Tides: Thermal and Gravitational, Gordon and Breach/Sci. Pub., 200, 1970. 8811
Charney, J. G.: Geostrophic turbulence, J. Atmos. Sci., 28, 1087–1095, 1971. 8835, 8836
Cohn, S. E. and Dee, D. P.: An analysis of the vertical structure equation for arbitrary thermal profiles, Q. J. Roy. Meteor. Soc., 115, 143–171, 1989. 8815, 8830
Daley, R.: Spectral characteristics of the ECMWF objective analysis system, ECMWF Tech. Rep. No. 40, 117, 1983. 8809
Daley, R.: Atmospheric data analysis, Cambridge University Press, Cambridge, UK, 460, 1991. 8809
Dee, D. P., Uppala, S. M., Simmons, A. J., Berrisford, P., Poli, P., Kobayashi, S., Andrae, U., Balmaseda, M. A., Balsamo, G., Bauer, P., Bechtold, P., Beljaars, A. C. M., van de Berg, L., Bidlot, J., Bormann, N., Delsol, C., Dragani, R., Fuentes, M., Geer, A. J., Haimberger, L., Healy, S. B., Hersbach, H., Hólm, E., Isaksen, L., Kållberg, P., Köhler, M., Matricardi, M., McNally, A. P., Monge-Sanz, B. M., Morcrette, J.-J., Park, B.-K., Peubey, C., de Rosnay, P., Tavolato, C., Thépaut, J.-N., and Vitart, F.: The ERA-Interim reanalysis: configuration and performance of the data assimilation system, Q. J. Roy. Meteor. Soc., 137, 553–597–1841, 2011. 8809, 8810, 8835
Dikii, L. A.: The terrestrial atmosphere as an oscillating system, (translated by C. M. Wade) Izv. Acad. Sci. USSR, Atmos. Ocean. Phys., 1, 469–489, 1965. 8819
Errico, R. M.: On the removal of gravitational noise in numerical forecasts, J. Meteorol. Soc. Jpn., 75, 219–227, 1997. 8808
Flattery, T. W.: Hough functions., Tech. Rep. 21, Dept. Geophys. Sci., University of Chicago, 175 pp., 1967. 8819
Frehlich, R. and Sharman, R.: The use of structure functions and spectra from numerical model output to determine effective model resolution, Mon. Weather Rev., 136, 1537–1553, 2008. 8836
Geisler, J. E. and Stevens, D. E.: On the vertical structure of damped steady circulation in the tropics, Q. J. Roy. Meteor. Soc., 108, 87–93, 1982. 8841

GMDD
7, 8805–8873, 2014

Gill, A. E.: Some simple solution for heat-induced tropical circulation, Q. J. Roy. Meteor. Soc., 106, 447–462, 1980. 8808, 8830, 8841
Hartman, D. L.: The atmospheric general circulation and its variability, J. Meteorol. Soc. Jpn., 85B, 123–143, 2007. 8838
Hayashi, J.: Space-time spectral analysis and its applications to atmospheric waves, J. Meteorol. Soc. Jpn., 60, 156–171, 1981. 8830
Heckley, W. A. and Gill, A. E.: Some simple analytical solutions to the problem of forced equatorial long waves, Q. J. Roy. Meteor. Soc., 110, 203–217, 1984. 8830
Hildebrand, F. B.: Methods of Applied Mathematics., Prentice-Hall, Inc., 1958. 8814
Hough, S. S.: On the application of harmonic analysis to the dynamical theory of the tides – Part II. On the general integration of Laplaceś dynamical equations., Philos. Tr. R. Soc. S-A, 191, 139–185, 1898. 8819
Jacobs, S. J. and Wiin-Nielsen, A.: On the stability of a barotropic basic flow in a stratified atmosphere, J. Atmos. Sci., 23, 682–687, 1966. 8813
Kasahara, A.: Various vertical coordinate systems used for numerical weather prediction, Mon. Weather Rev., 102, 509–522, 1974 (Corrigendum, Mon. Weather Rev., 103, 664, 1975). 8811
Kasahara, A.: Normal modes of ultralong waves in the atmosphere, Mon. Weather Rev., 104, 669–690, 1976. 8819
Kasahara, A.: Further studies on a spectral model of the global barotropic primitve equations with Hough harmonic expansions, J. Atmos. Sci., 35, 2043–2051, 1978. 8820
Kasahara, A.: Effect of zonal flows on the free oscillations of a barotropic atmosphere, J. Atmos. Sci., 37, 917–929, 1980 (Corrigendum, J. Atmos. Sci., 38, 2284–2285, 1981). 8821
Kasahara, A.: The linear response of a stratified global atmosphere to a tropical thermal forcing, J. Atmos. Sci., 41, 2217–2237, 1984. 8809, 8841
Kasahara, A. and Puri, K.: Spectral representation of three-dimensional global data by expansion in normal mode functions, Mon. Weather Rev., 109, 37–51, 1981. 8807, 8809, 8810
Kasahara, A. and Tanaka, H.: Application of vertical normal mode expansion to problems of baroclinic instability, J. Atmos. Sci., 46, 489–510, 1989. 8808
Kim, J. E. and Alexander, M. J.: Tropical precipitation variability and convectively coupled equatorial waves on submonthly time-scales in reanalyses and TRMM, J. Climate, 26, 3013–3030, 2013. 8808

GMDD
7, 8805–8873, 2014

Kleist, D. T., Parrish, D. F., Derber, J. C., Treadon, R., Errico, R. M., and Yang, R.: Improving incremental balance in the GSI 3DVAR analysis system, Mon. Weather Rev., 137, 1046–1060, 2009. 8808

Lamb, H.: Hydrodynamics, Dover Pub., 1932. 8811

Le Dimet, F.-X. and Talagrand, O.: Variational algorithms for analysis and assimilation of meteorological observations: theoretical aspects, Tellus A, 38, 97–110, 1986. 8808

Lilly, D. K.: Lectures in sub-synoptic scales of motion and two-dimensional turbulence, in: Dynamic Meteorology, edited by: Morel, P., 1973. 8836

Lin, J.-L., Kiladis, G., Mapes, B. E., Weickmann, K. M., Sperber, K. R., Lin, W., Wheeler, M. C., Schubert, S. D., Genio, A. D., Donner, L. J., Emori, S., Gueremy, J.-F., Hourdin, F., Rasch, P. J., Roeckner, E., and Scinocca, J. F.: Tropical intraseasonal variability in 14 IPCC AR4 climate models. Part I: Convective signals, J. Climate, 19, 2665–2690, 2006. 8808, 8810, 8842

Longuet-Higgins, M. S.: The eigenfunctions of Laplaceś tidal equations over a sphere, Philos. Tr. R. Soc. S-A, 262, 511–607, 1968. 8819

Lorenz, E. N.: Available potential energy and the maintenance of the general circulation, Tellus, 7, 157–167, 1955. 8824

Lynch, P. and Huang, X.-Y.: Initialization of the HIRLAM model using a digital filter, Mon. Weather Rev., 120, 1019–1034, 1992. 8808

Machenhauer, B.: On the dynamics of gravity oscillations in a shallow water model, with applications to normal mode initialization, Beitr. Phys. Atmos., 50, 253–271, 1977. 8808

Madden, R. A.: Large-scale, free Rossby waves in the atmosphere – an update., Tellus A, 59, 571–590, 2007. 8808

Majda, A. J., Khouider, B., Kiladis, G., Straub, K., and Shefter, M.: A model for convectively coupled tropical waves: nonlinearity, rotation, and comparison with observations, J. Atmos. Sci., 61, 2188–2205, 2004. 8841

Margules, M.: Air motions in a rotating spheroidal shell, Max Margules wrote three papers, “Luftbewegungen in einer rotierenden Sphäroidschale bei zonaler Druckverteilung”, Sitz.-Ber. kaiserl. Akad. Wissensch. Wien, Math.-Nat. Cl., Abt. IIa, vol. 101 (1892), 597–626, “Luftbewegungen in einer rotierenden Sphäroidschale (II. Theil)”, Ibid., vol. 102 (1893), 11–56, and “Luftbewegungen in einer rotierenden Sphäroidschale (III. Theil)”, Ibid., vol. 102 (1893), 1369–1421. These three articles were translated by B. Haurwitz as an NCAR technical re-

GMDD
7, 8805–8873, 2014

port “Air motions in a rotating spheroidal shell”, NCAR/TN-156+STR, National Center for Atmospheric Research, Boulder, CO, 1892. 8819
Marques, C. A. F. and Castanheira, J. M.: A detailed normal-mode energetics of the general circulation of the atmosphere, J. Atmos. Sci., 69, 2718–2732, 2012. 8808
Matsuno, T.: Quasi-geostrophic motions in the equatorial area, J. Meteorol. Soc. Jpn., 44, 25–42, 1966. 8820, 8830
Nastrom, G. D. and Gage, K. S.: A climatology of aircraft wavenumber spectra observed by commercial aircraft, J. Atmos. Sci., 42, 950–960, 1985. 8836
Phillips, N. A.: A coordinate system having some special advantages for numerical forecasting, J. Meteor., 14, 184–185, 1957. 8811
Phillips, N. A.: Dispersion processes in large-scale weather prediction, Sixth IMO Lecture, World Meteorological Organization, No. 700, 1990. 8819
Platzman, G. W.: Two-dimensional free oscillations in natural basins, J. Phys. Oceanogr., 2, 117–138, 1972. 8818
Platzman, G. W.: Comments on the origin of the energy product, B. Am. Meteorol. Soc., 73, 1847–1851, 1992. 8823
Shigehisa, Y.: Normal modes of the shallow water equations for zonal wavenumber zero, J. Meteorol. Soc. Jpn., 61, 479–493, 1983. 8820
Shutts, G. J. and Vosper, S. B.: Stratospheric gravity waves revealed in NWP model forecasts, Q. J. Roy. Meteor. Soc., 137, 303–317, 2011. 8841
Siebert, M.: Atmospheric tides, Adv. Geophys., 7, 105–187, 1961. 8819
Simons, T. J.: A three-dimensional spectral prediction equation, Atmos. Sci. Paper No. 127, Dept. Atmos. Sci., Colorado State Univ., 1968. 8813
Staniforth, A., Beland, M., and Coté, J.: An analysis of the vertical structure equation in sigma coordinates, Atmos. Ocean, 23, 323–358, 1985. 8809, 8830
Swarztrauber, P. N. and Kasahara, A.: The vector harmonic analysis of Laplace tidal equations, SIAM J. Stat. Comput., 6, 464–491, 1985. 8820, 8826
Tanaka, H.: Global energetics analysis by expansion into three-dimensional normal-mode functions during the FGGE winter, J. Meteorol. Soc. Jpn., 63, 180–200, 1985. 8807
Tanaka, H. and Kimura, K.: Normal-Mode Energetics Analysis and the Intercomparison for the Recent ECMWF, NMC, and JMA Global Analyses, J. Meteorol. Soc. Jpn., 74, 525–538, 1996. 8808

GMDD
7, 8805–8873, 2014

Tanaka, H. and Kung, E.: Normal-mode expansion of the general circulation during the FGGE year, J. Atmos. Sci., 45, 3723–3736, 1988. 8807

Tanaka, H. and Terasaki, K.: Blocking formation by an accumulation of barotropic energy exceeding the rossby wave saturation level at the spherical Rhines scale, J. Meteorol. Soc. Jpn., 84, 319–332, 2006. 8808

Taylor, G. I.: The oscillations of the atmosphere, Proc. R. Soc. Lon. Ser.-A, 156, 318–326, 1936. 8812, 8813

Terasaki, K. and Tanaka, H.: An analysis of the 3-D atmospheric energy spectra and interactions using analytical vertical structure functions and two reanalyses, J. Meteorol. Soc. Jpn., 85, 785–796, 2007. 8809

Tung, K. K. and Orlando, W. W.: The k^{-3} and $k^{-5/3}$ energy spectrum of atmospheric turbulence: quasigeostrophic two-level simulation, J. Atmos. Sci., 60, 824–835, 2003. 8836

Wergen, W.: The diabatic ECMWF normal mode initialization scheme, Beitr. Phys. Atmos., 61, 274–302, 1988. 8808

Wheeler, M. and Kiladis, G. N.: Convectively coupled equatorial waves: analysis of clouds and temperature in the wavenumber-frequency domain, J. Atmos. Sci., 56, 374–399, 1999. 8808, 8820, 8830

Williamson, D. L. and Dickinson, R. E.: Free oscillations of the NCAR global circulation model, Mon. Weather Rev., 104, 1372–1391, 1976. 8841

Yang, G.-Y., Hoskins, B. J., and Slingo, J.: Convectively coupled equatorial waves: A new methodology for identifying wave structures in observational data, J. Atmos. Sci., 60, 1637–1654, 2003. 8808

Žagar, N., Tribbia, J., Anderson, J. L., and Raeder, K.: Uncertainties of estimates of inertio-gravity energy in the atmosphere. Part I: Intercomparison of four analysis datasets, Mon. Weather Rev., 137, 3837–3857. Corrigendum, Mon. Weather Rev., 138, 2476–2477, 2009a. 8807, 8809, 8831, 8835, 8836

Žagar, N., Tribbia, J., Anderson, J. L., and Raeder, K.: Uncertainties of estimates of inertio-gravity energy in the atmosphere. Part II: Large-scale equatorial waves, Mon. Weather Rev., 137, 3858–3873. Corrigendum, Mon. Weather Rev., 138, 2476–2477, 2009b. 8835, 8836, 8837, 8841, 8842

Žagar, N., Tribbia, J., Anderson, J. L., and Raeder, K.: Balance of the background-error variances in the ensemble assimilation system DART/CAM, Mon. Weather Rev., 139, 2061–2079, 2011. 8807

GMDD

7, 8805–8873, 2014

Žagar, N., Terasaki, K., and Tanaka, H.: Impact of the vertical discretization of analysis data on the estimates of atmospheric inertio-gravity energy, Mon. Weather Rev., 140, 2297–2307, 2012. 8807

Žagar, N., Isaksen, L., Tan, D., and Tribbia, J.: Balance and flow-dependency of background-error variances in the ECMWF 4D-Var ensemble, Q. J. Roy. Meteor. Soc., 139, 1229–1238, doi:10.1002/qj.2033, 2013. 8807, 8810

GMDD

7, 8805–8873, 2014

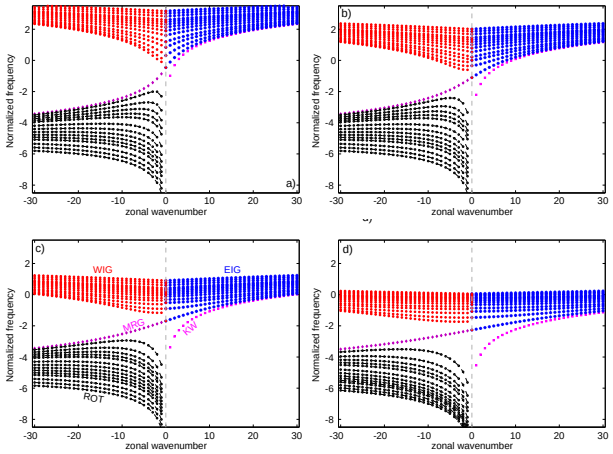

Figure 1. Frequencies of spherical normal modes for different equivalent depths. **(a)** D = 10 km, **(b)** D = 1 km, **(c)** D = 100 m and **(d)** D = 10 m. Frequencies are normalized by 2Ω factor and shown in logarithmic scale. Frequencies of the easterly and westerly inertia-gravity modes (EIG and WIG, respectively) are shown for the meridional modes n equal 0, 1, 3, 6, 9, 14, 19, 24, 29, 34, 39, 49, 59 and 69. For the balanced modes (ROT), shown are meridional modes n = 0, 1, 3, 5, 7, 9, 14, 19, 24, 29, 34, 39, 49, 59 and 69. Frequencies of the Kelvin modes (n = 0 EIG) and mixed Rossby-gravity modes (n = 0 ROT) are shown by magenta-coloured symbols. Frequencies of ROT modes $n > 1$ are denoted by gray circles and interconnected by dashed black lines. For the EIG and WIG modes frequencies are shown by blue and red symbols, respectively. Negative frequencies correspond to negative values of zonal wavenumbers. Frequencies for k = 0 are zero for all ROT modes, for the MRG mode, for the Kelvin mode and for the n = 0 WIG mode and therefore do not appear in the figures. For $n > 0$ and k = 0, frequencies of the WIG modes have opposite sign and equal values as frequencies of the EIG modes. For $k > 1$, frequencies of the WIG modes have larger absolute values than frequencies of the EIG modes for the same n.

GMDD
7, 8805–8873, 2014

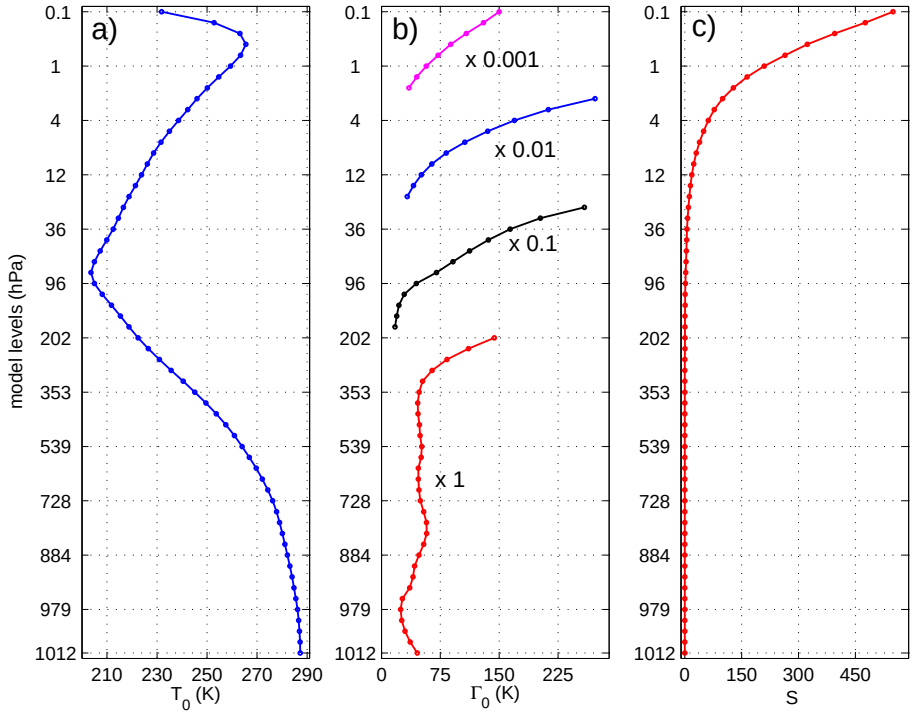

Figure 2. Globally-averaged vertical profiles of **(a)** temperature, **(b)** stability Γ_0 and **(c)** normalized stability parameter S on model levels which is input to the vertical structure equation (10). Profiles are based on ERA Interim model-level data for year 2000. Labels on y axis are average pressures of the model levels. Values of stability at various levels in **(b)** are scaled by different factors for clarity reasons. Under 200 hPa stability is not scales.

GMDD
7, 8805–8873, 2014

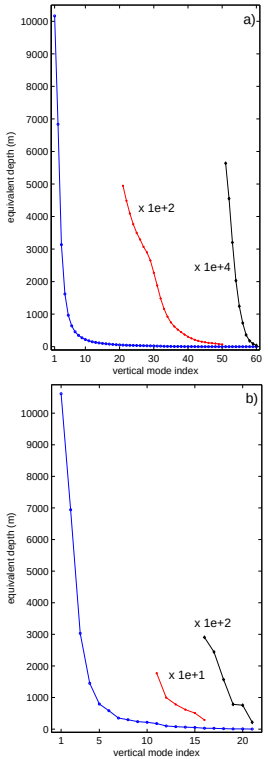

Figure 3. Values of the equivalent depths obtained as solution of the vertical structure equation for ERA Interim modelling system. **(a)** 60 model levels and **(b)** 21 model levels closest to the standard 21 pressure levels. A part of equivalent depths in **(a)** is also shown multiplied by factor 100 (modes 21–50) and by factor 10 000 (modes 51 to 60). A part of equivalent depths in **(b)** is similarly multiplied by factor 10 (modes 11–16) and by factor 100 (modes 16 to 21).

GMDD
7, 8805–8873, 2014

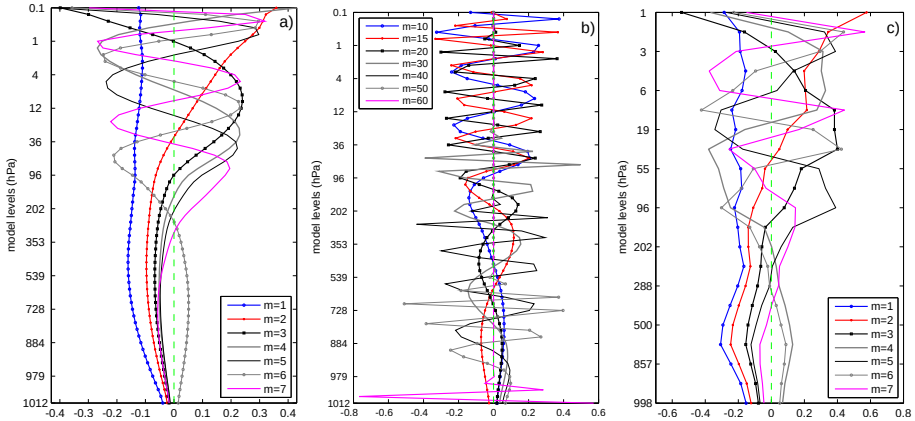

Figure 4. Vertical structure functions for **(a)** first seven vertical modes and **(b)** modes 10, 15, 20, 30, 40 50 and 60, derived for 60 model levels of ERA Interim. **(c)** As **(a)** but for the case of 21 model levels closest to the standard 21 pressure levels.

GMDD
7, 8805–8873, 2014

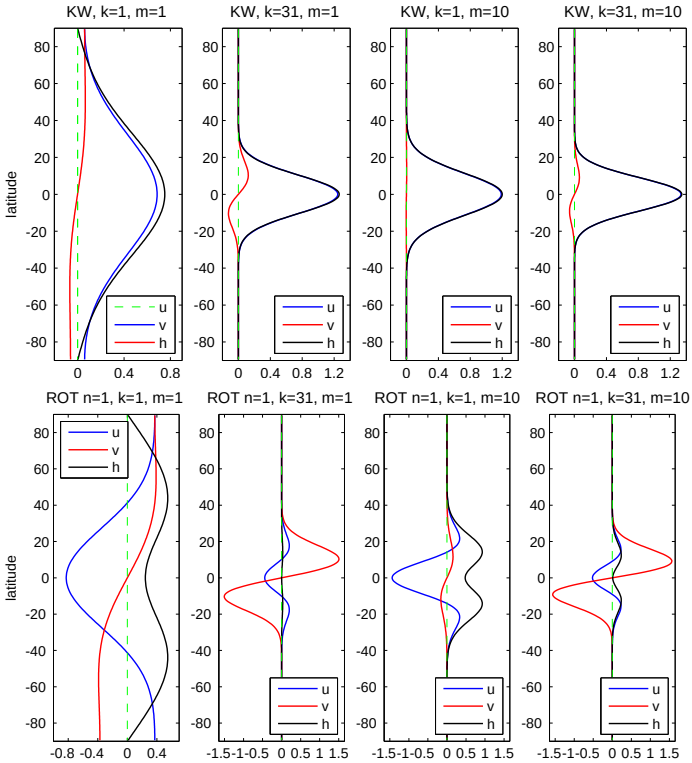

Figure 5. Meridional structure of the Hough harmonics for (top) Kelvin mode and (bottom) $n = 1$ balanced mode. Four panels for each mode correspond to various combinations of the zonal wavenumber k and vertical mode m, as defined in panels' title.

GMDD
7, 8805–8873, 2014

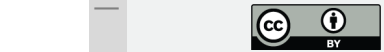

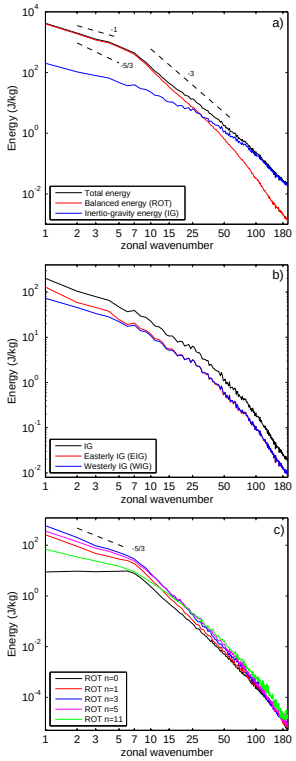

Figure 6. Atmospheric energy spectra. **(a)** Energy distribution in balanced (red line) and inertio-gravity (blue line) motions and their sum (total wave energy, in black) as a function of the zonal wavenumber. **(b)** As **(a)** but IG (black), EIG (red) and WIG (blue). **(c)** As **(a)** but balanced spectra for meridional modes $n = 0$, 1, 3, 5, 11. Spectra are obtained by averaging 30 years of outputs from ERA Interim, 12:00 UTC analysis. Summation is performed over **(a, b)** all (m, n) and **(c)** all m and the mean state ($k = 0$) is not included. Short dashed lines (black) correspond to the spectra with slopes -3, -1 and $-5/3$ as written next to the lines.

GMDD
7, 8805–8873, 2014

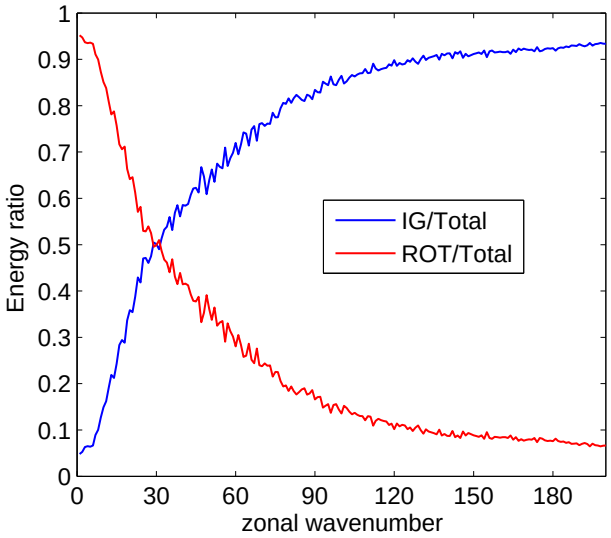

Figure 7. Ratio of balanced (red line) and inertio-gravity (blue line) energy and total energy in each zonal wavenumber. Averaging is performed for 30 year period and for all (m, n).

GMDD
7, 8805–8873, 2014

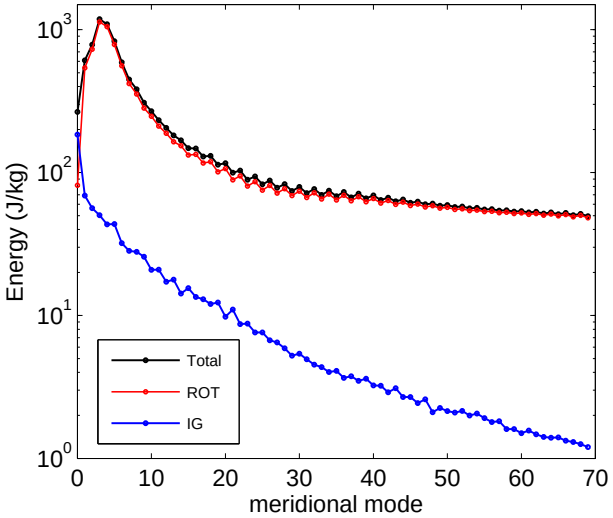

Figure 8. Distribution of total, balanced and inertio-gravity wave energy in meridional modes. Summation is performed over all (m, k) and the mean state ($k = 0$) is not included.

GMDD
7, 8805–8873, 2014

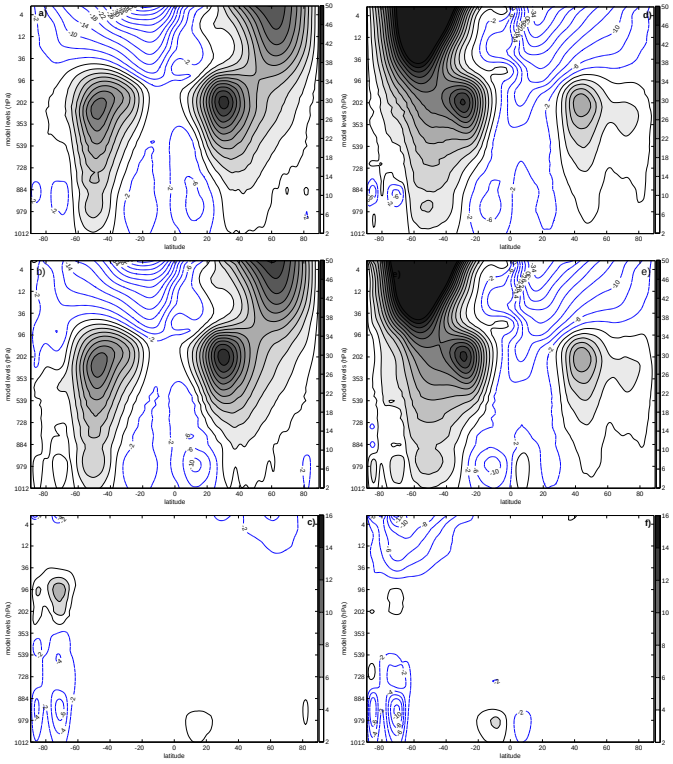

Figure 9. Meridional profile of the zonally-averaged **(a, d)** total, **(b, e)** balanced and **(c, f)** unbalanced components of the zonal wind in **(a–c)** January and **(d–f)** July. Westerlies are shaded while easterlies are drawn by blue isolines. Contour interval is $4\,\mathrm{m\,s^{-1}}$ for balanced and $2\,\mathrm{m\,s^{-1}}$ for IG speeds.

GMDD
7, 8805–8873, 2014

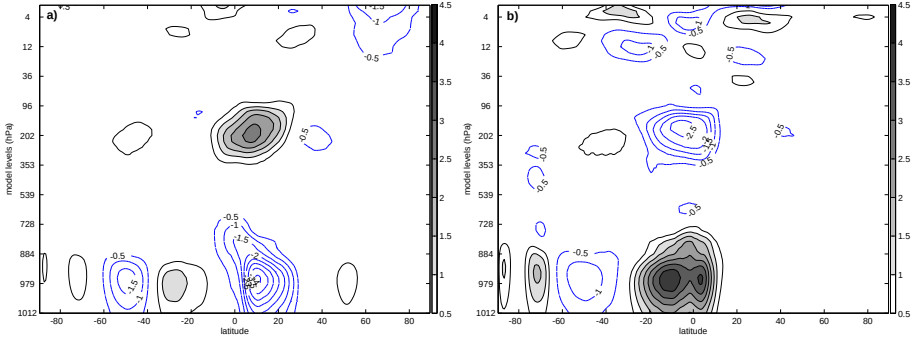

Figure 10. As in Fig. 9 but for the IG component of the zonally-averaged meridional wind. **(a)** January and **(b)** July. Contour interval is 0.5 m s^{-1}.

GMDD
7, 8805–8873, 2014

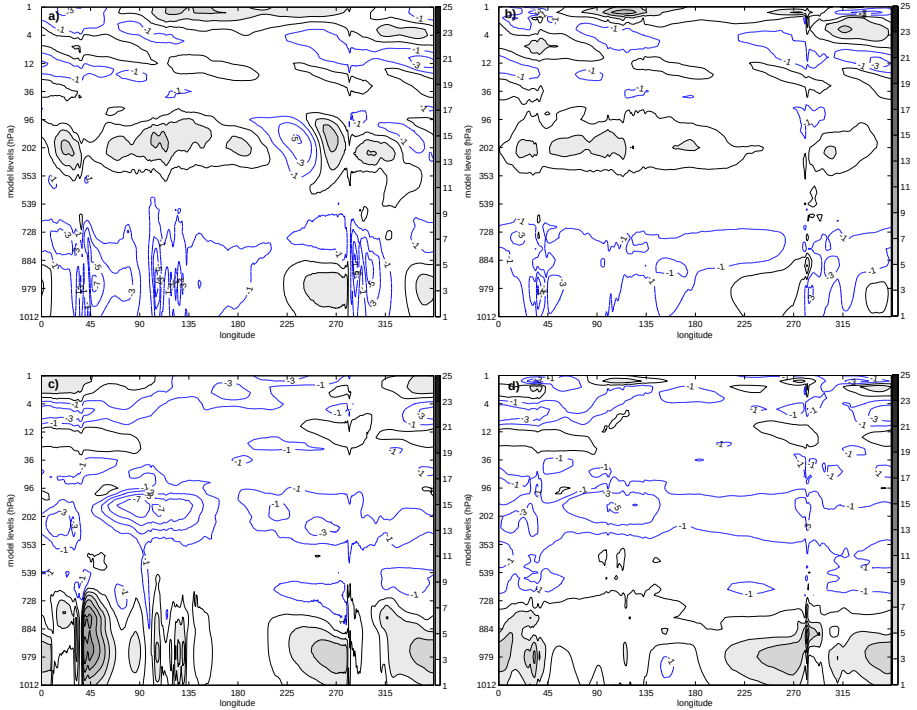

Figure 11. Meridional winds along the equator in **(a, b)** January and **(c, d)** July. **(a, c)** All modes and **(b, d)** unbalanced modes. Spacing is every 2 m s^{-1} with positive values (northerly wind) shaded and negative values (southerly wind) in blue.

GMDD
7, 8805–8873, 2014

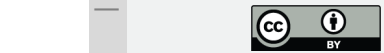

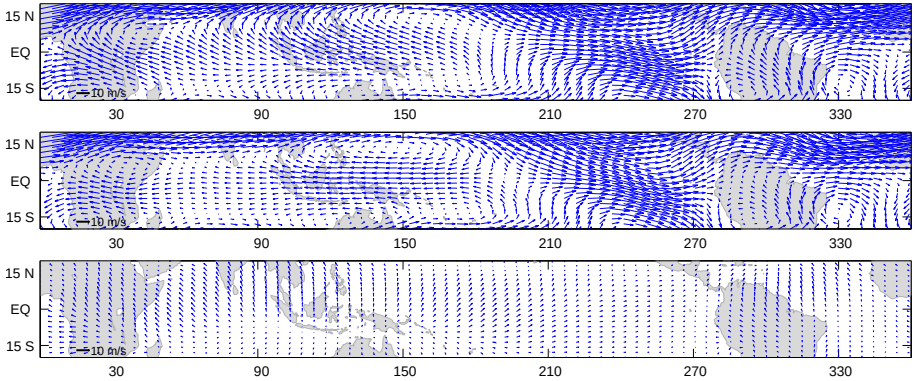

Figure 12. ERA Interim horizontal winds in January on model level 31 (about 229 hPa) for (top) total circulation, (middle) balanced circulation and (bottom) unbalanced circulation. Wind vectors in all panels are scaled by the same factor and drawn every three and seven grid points in the zonal and meridional directions, respectively.

GMDD
7, 8805–8873, 2014

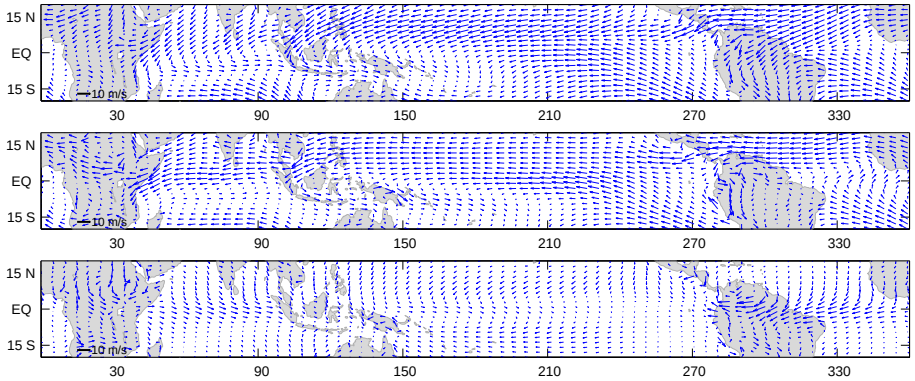

Figure 13. As in Fig. 12 but for the model level 51 (about 909 hPa).

GMDD
7, 8805–8873, 2014

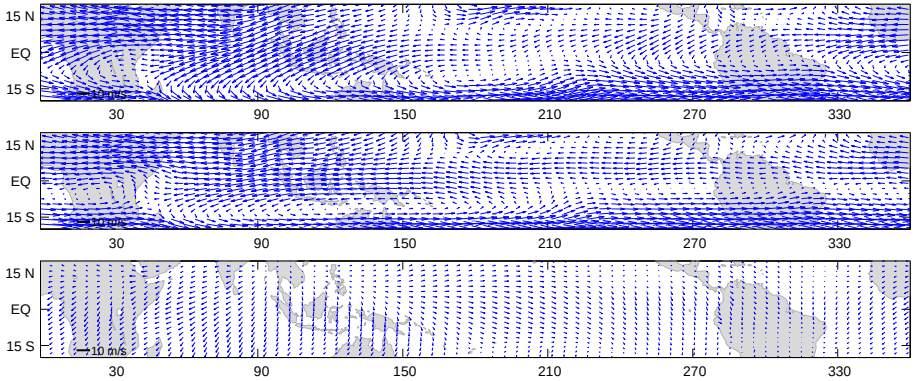

Figure 14. As in Fig. 12 but for July.

GMDD
7, 8805–8873, 2014

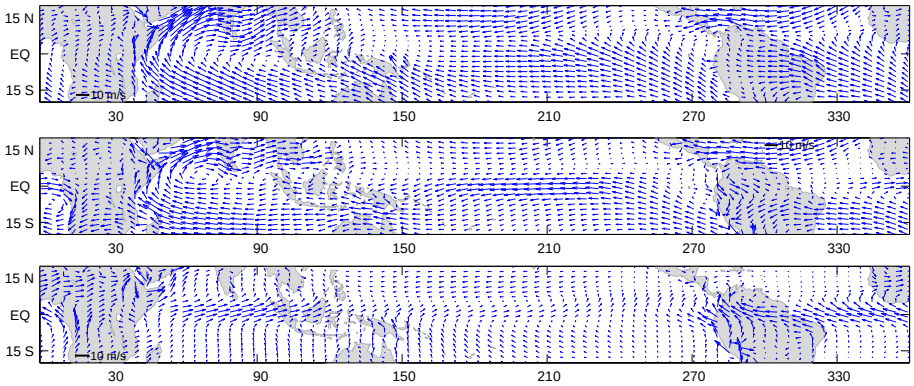

Figure 15. As in Fig. 13 but for July.

GMDD
7, 8805–8873, 2014

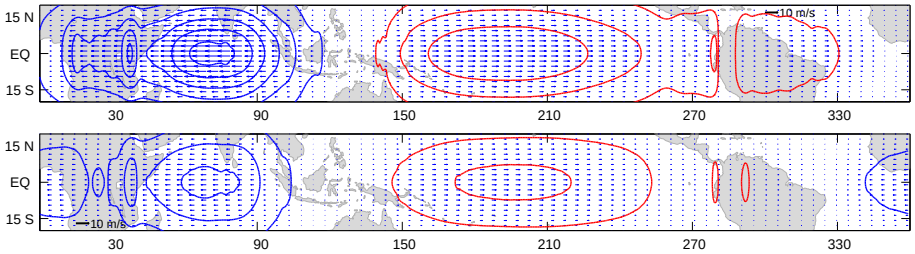

Figure 16. ERA Interim climatology of Kelvin wave winds and geopotential height perturbations for July on (upper panel) model level 27, at about 133 hPa and (panel below) and model level 31, at about 229 hPa. Isolines for the geopotential height are drawn every 10 m, starting from ±10 m with positive values in red and negative in blue.

GMDD
7, 8805–8873, 2014